International
Progress Report

IPR-02-24

Äspö Hard Rock Laboratory

Prototype Repository

Prediction analysis A for the PRP with the numerical code THAMES

Yutaka Sugita
Akira Ito
Japan Nuclear Cycle Development Institute

Masakazu Chijmatsu
Hazama Corporation

Hiroshi Kurikami
Kyoto University

May 2002

Svensk Kärnbränslehantering AB
Swedish Nuclear Fuel
and Waste Management Co
Box 5864
SE-102 40 Stockholm Sweden
Tel +46 8 459 84 00
Fax +46 8 661 57 19

Äspö Hard Rock
Laboratory

Report no.	No.
IPR-02-24	F63K
Author	Date
Sugita, Chijmatsu, Kurikami	02-05-31
Checked by	Date
Roland Pusch	02-06-10
Approved	Date
Christer Svemar	02-06-30

Äspö Hard Rock Laboratory

Prototype Repository

Prediction analysis A for the PRP with the numerical code THAMES

Yutaka Sugita
Akira Ito
Japan Nuclear Cycle Development Institute

Masakazu Chijmatsu
Hazama Corporation

Hiroshi Kurikami
Kyoto University

May 2002

Keywords: Prototype Repository, numerical modelling, numerical code, THM processes, THAMES, MX-80, backfill

Abstract

This report describes the prediction analysis results performed by JNC as one work package (WP) for the prototype repository project (PRP). JNC has the numerical code THAMES for analysis of the coupled phenomena in and around the engineered barrier system on the high level radioactive waste repository.
JNC has performed the WP3h of the prediction analysis of the coupled Thermal, Hydraulic and Mechanical (THM) behaviour in and around the test holes of the PRP.

Sammanfattning

Denna rapport presenterar resultaten från den prediktionsanalys som JNC har gjort i form av ett arbetspaket (Work Package – WP) för Prototypförvarsprojektet (PRP). JNC använder den numeriska koden THAMES för analys av de kopplade processerna i och omkring ingenjörsbarriärerna i ett slutförvar för högaktivt avfall.

JNC har gjort WP3h rörande prediktionsanalys av de kopplade termo-hydro-mekaniska förloppen (THM) i och omkring PRP:s testhål.

Summary

In this report, we carried out the pre-analysis of Prototype Repository by two-dimensional model. From the pre-analysis, following results are obtained.

1) Re-saturation phenomena in the buffer are not dependent on the permeability of rock mass if the hydraulic conductivity of rock mass is in the 10^{-10} to 10^{-14}m/s range.

2) The re-saturation time of the buffer is between 6,000 days and 20,000 days. It is dependent on the initial void ratio of the buffer.

3) There is not so large difference about the temperature distribution between the some cases for modelling of the gap compared with the distribution of degree of saturation in the buffer.

4) It is important to evaluate the water movement due to thermal effect in order to estimate the re-saturation phenomena in the buffer mass.

5) It is concluded that when gap is not considered in the model it is better to use the property at the high density of bentonite before installing into the disposal pit. However, these are the results when we did not consider the structure change inside the bentonite due to the swelling in detail. In order to achieve the more detail evaluation, it needs to consider the structure change inside the bentonite and the parameter change during the swelling.

In this report, we investigated the effect of void ratio and thermal vapor flow diffusivity of the buffer and the effect of the permeability of surrounding rock on the re-saturation phenomena in the buffer by two-dimensional model. Next stage, we will investigate the effect of exist of adjacent boreholes by three-dimensional model.

Tables of contents

List of Tables

List of Figures

1 Introduction

Prototype Repository Project (PRP) is one project performed at Äspö Hard Rock Laboratory (HRL) to demonstrate a deep repository in crystalline rock under natural and realistic condition. The PRP has many WP.

JNC takes part in WP3h of the PRP. JNC contributes the prediction of the coupled thermo-hydro-mechanical behaviour in and around the engineered barrier system (EBS). JNC will perform two kind of the prediction of the coupled behaviour. Prediction A is analysed with two dimensional analysis model, prediction B will be done with 3 dimensional analysis model. This report summarised the results of the prediction A.

2 Description of the numerical code THAMES

JNC has developed the coupled thermal, hydraulic and mechanical numerical analysis code. This analysis code considers the behaviour of a saturated-unsaturated medium. This code has validated with the data of the laboratory tests (Chijimatsu, et al, 1998), the engineered scale tests (Chijimatsu, et al, 2000a) and the in-situ experiments (Chijimatsu, et al, 2000b).

2.1 Analysis objective

Analysis of the coupled thermal, hydraulic and mechanical process is carried out with the computer code named THAMES (Ohnishi, et al, 1985). THAMES is a finite element code for analysis of coupled thermal, hydraulic and mechanical behaviours of a saturated-unsaturated medium. THAMES is extended to take account of the behaviour in the buffer materials such as the water flow due to thermal gradient and the swelling phenomena. The unknown variables are total pressure, displacement vector and temperature. The quadratic shape function is used for the displacements and linear one is used for total pressure and temperature.

2.2 Governing equations of coupled THM process

The mathematical formulation for the model utilises Biot's theory, with the Duhamel-Neuman's form of Hooke's law, and energy balance equation. The governing equations are derived with the fully coupled thermal, hydraulic and mechanical relationships.

1) Assumption

The governing equations are derived under the following assumptions:

(1) The medium is poro-elastic.

(2) Darcy's law is valid for the flow of water through a saturated-unsaturated medium.

(3) Heat flow occurs only in solid and liquid phases. The phase change of water from liquid to vapor is not considered.

(4) Heat transfer among three phases (solid, liquid and gas) is disregarded.

(5) Fourier's law holds for heat flux.

(6) Water density varies depending upon temperature and the pressure of water

2) Equilibrium equation

The equation of motion for a medium in a static case is known as an equilibrium equation. It is written in a total stress expression as

$$\sigma_{ij,j} + \rho b_i = 0 \tag{1}$$

where σ_{ij} is the stress, ρ is the density of as soil-water mixing medium and b_i is the body force.

Terzaghi defined the effective stress principle. Bishop and Blight extended his definition and proposed the following equation for a saturated-unsaturated medium:

$$\sigma_{ij} = \sigma'_{ij} + \chi \delta_{ij} \rho_f g \psi \tag{2}$$

where σ'_{ij} is the effective stress, δ_{ij} is the Kronecker's delta, ρ_f is the unit weight of water, g is the acceleration of gravity and ψ is the pressure head. Subscript f means "fluid". Parameter χ is defined as

$$\chi = 1 \text{ (Saturated zone)}, \quad \chi = \chi(S_r) \text{ (Unsaturated zone)} \tag{3}$$

χ is a nonlinear function of S_r (the degree of saturation).

The validity of equation (2) is not definite and is still under debate even now. However, here it is assumed that equation (2) holds and that χ is approximately equal to S_r .

Substituting equation (1) for equation (2), the equilibrium equation for the effective stress is a saturated-unsaturated geologic medium is obtained, namely,

$$\left(\sigma'_{ij} + \chi \delta_{ij} \rho_f g \psi\right)_{,j} + \rho b_i = 0 \tag{4}$$

where ($\chi \delta_{ij} \rho_f g \psi$) is a term which means that changes in the pressure head influence the equilibrium equation.

The effects of temperature can be implemented in a constitutive law for a sold medium. For an isotropic linear elastic material, Duhamel-Neuman's relationship can be used and the following constitutive law is obtained:

$$\sigma_{ij}^{\copyright} = C_{ijkl}\varepsilon_{kl} - \beta\delta_{ij}(T - T_o) \tag{5}$$

where $\beta = (3\lambda+2\mu)\alpha_T$. C_{ijkl} is the elastic matrix, ε_{kl} is the strain tensor, T is the temperature, λ and μ are Lamé's constant and α_T is the thermal expansivity coefficient. Subscript o means that the parameter is in a reference state.

The infinitesimal strain-deformation relationship is

$$\varepsilon_{kl} = \frac{1}{2}(u_{k,l} + u_{l,k}) \tag{6}$$

where u_i is the deformation vector.

Substituting equation (5) and (6) into equation (4), the stress equilibrium equation is obtained. It takes into account the effects of temperature and pore pressure change, namely,

$$\left[\frac{1}{2}C_{ijkl}(u_{k,l} + u_{l,k}) - \beta\delta_{ij}(T - T_o) + \chi\delta_{ij}\rho_f g\psi\right]_{,j} + \rho b_i = 0 \tag{7}$$

$(-\beta\delta_{ij}(T-T_o))_{,j}$ is a term which stands for the influence of heat transfer on the equilibrium equation.

3) Continuity equation for ground water

The equation of continuity for ground water in a saturated-unsaturated zone is derived from Richards' theory as follow:

$$\frac{\partial(\rho_f\theta)}{\partial t} = -(\rho_f v_i)_{,i} \tag{8}$$

where θ is the volumetric water content, t is the time and v_i is the velocity vector.

The equation of motion for ground water can be explained by Darcy's law. That is,

$$v_i = -k(\theta)_{ij}h_{,j} \tag{9}$$

where $k(\theta)_{ij}$ is the permearbility tensor that is a function of θ. h is the total head.

The total head can be expressed as the sum of pressure head ψ and elevation head z.

$$h = \psi + z \tag{10}$$

The volumetric water content θ is a function of the degree of saturation S_r and porosity n, which is expressed as,

$$\theta = n \ S_r \tag{11}$$

Substitution equations (9), (10) and (11) into (8), following equation is obtained.

$$\left\{ \rho_f \ k(\theta)_{ij} \ (\psi + z)_{,j} \right\}_{,i} = \frac{\partial}{\partial t} \rho_f \ n \ S_r \tag{12}$$

The right-hand side of equation (12) is expanded to

$$\frac{\partial}{\partial t} \rho_f \ n \ S_r = n \ S_r \frac{\partial \rho_f}{\partial t} + \rho_f \ S_r \frac{\partial n}{\partial t} + \rho_f \ n \frac{\partial S_r}{\partial t} \tag{13}$$

The first term at the right-hand side represents a density change in the pore water. The second term means a change in the skeleton of the porous medium. The third term stands for a change in the degree of saturation in an unsaturated region.

Considering the compressibility and the thermal expansivity of water, the density of water can be expressed as,

$$\rho_f = \rho_{fo} \left[1 - \beta_T (T - T_o) + \beta_P (P - P_o) \right] \tag{14}$$

where P is the pore water pressure and ρ_{fo} is the reference density at $P=P_o$ and $T=T_o$.

β_T and β_P are the thermal expansivity and the compressibility of water, respectively,

$$\beta_T = \left| -\frac{1}{\rho_f}\frac{\partial \rho_f}{\partial T} \right| \quad (P = \text{constant}) \tag{15}$$

and

$$\beta_P = \left| \frac{1}{\rho_f}\frac{\partial \rho_f}{\partial P} \right| \quad (T = \text{constant}) \tag{16}$$

Eaton assumed that buoyancy could be ignored in an unsaturated zone due to its insignificant effect on the fluid flow. Adopting this assumption, β_T is set to be zero in an unsaturated zone.

A combination of the first terms in equations (13) and (14) yields

$$n\ S_r \frac{\partial \rho_f}{\partial t} = \rho_{fo}\ n\ S_r \left(-\beta_T \frac{\partial T}{\partial t} + \beta_P \frac{\partial P}{\partial t} \right) \tag{17}$$

Pressure head ψ is related to the pore water pressure as follows:

$$\psi = \frac{P}{\rho_f\ g} \tag{18}$$

Taking equation (10) and (18) into account, equation (17) can then be modified to

$$n\ S_r \frac{\partial \rho_f}{\partial t} = \rho_{fo}\ n\ S_r \left(-\beta_T \frac{\partial T}{\partial t} + \rho_f\ g\ \beta_P \frac{\partial \psi}{\partial t} \right) \tag{19}$$

Assuming that the strain is infinitesimal, the second and third terms at the right-hand side of equation (13) are expressed as

$$\rho_f\ S_r \frac{\partial n}{\partial t} \cong \rho_f\ S_r \frac{\partial u_{i,i}}{\partial t}$$

$$\rho_f\ n \frac{\partial S_r}{\partial t} \cong \rho_f \frac{\partial \left(n\ S_r \right)}{\partial t} = \rho_f \frac{\partial \theta}{\partial t} = \rho_f \frac{\partial \theta}{\partial \psi}\frac{\partial \psi}{\partial t} \tag{20}$$

Equation (12) is modified by using equation (19) and (20) as follows:

$$\left\{\rho_f k(\theta)_{ij} h_{,j}\right\}_{,i} - \rho_{fo} n S_r \rho_f g \beta_P \frac{\partial \psi}{\partial t} - \rho_f \frac{\partial \theta}{\partial \psi}\frac{\partial \psi}{\partial t} - \rho_f S_r \frac{\partial u_{i,i}}{\partial t} + \rho_{fo} n S_r \beta_T \frac{\partial T}{\partial t} = 0 \tag{21}$$

Equation (21) is an equation of continuity for ground water which takes into account the compressibility of the ground water and changes in density by temperature change.

4) Energy conservation law

In general, the ground consists of materials with three phases, i.e., solid, liquid and gas. It is not easy to understand the behaviour of heat transfer through such a composite material, because the way in which heat is transported is difficult for each phase and a heat transfer may occur between phases. However, the state of the gaseous phase in a ground is too complicated to be modelled. For simplicity, a pore in a porous medium is assumed to be filled with only a liquid phase here. This means that the ground water does not change in phase from liquid to gas or vise versa and that the thermal conductivity of the gaseous phase is disregarded. Since the heat conductivity of the gaseous phase is smaller than that of liquid and the solid phases, the heat conductivity of the composite material is not affected much by the volume of the gaseous phase.

An energy conservation law, based upon the process proposed by Bear and Carapcioglu, is derived for ground water from the above assumptions without the effect of viscous dissipation.

Consideration the existence of an unsaturated zone, the equation of energy conservation is written as,

$$nS_r \rho_f C_{vf}\left(\frac{\partial T_f}{\partial t} + V_f \nabla T_f\right) = -\nabla n S_r J_f - \left(\frac{\partial P}{\partial T_f}\right)_{\rho_f} n S_r T_f \nabla V_f \tag{22}$$

where C_v is the specific heat and J is the heat flux by conduction. In equation (22), the first term at the left-hand side shows the time dependency of energy, the second term shows the change in energy due to heat convection. The first term at the right-hand side express the change in energy by heat conduction and the second term shows the reversible energy change caused by compression.

Similarly, the energy conservation law for a solid phase is written as,

$$(1-n)\rho_s C_{vs}\left(\frac{\partial T_s}{\partial t} + V_s \nabla T_s\right) = -\nabla(1-n) J_s - (1-n)\beta T_s \frac{\partial \varepsilon_s}{\partial t} \tag{23}$$

where subscript s means solid. In equation (23), the second term at the right-hand side indicates the reversible energy change caused by deformation.

Faust and Mercer proposed that the movement of water through porous media is so slow and the surface areas of all phases are so large that it is reasonable to assume that a local thermal equilibrium among phase is achieved instantaneously. This means that the heat transfer between phases in the ground can be disregarded. If this assumption is permitted, the following equation is then valid:

$$T = T_s = T_f \tag{24}$$

Using this assumption, equations (22), (23) and (24) can be combined and an equation of energy conservation for the ground can be obtained by

$$\begin{aligned}&\left[nS_r\rho_f C_{vf} + (1-n)\rho_s C_{vs}\right]\frac{\partial T}{\partial t} + \left[nS_r\rho_f C_{vf}V_f + (1-n)\rho_s C_{vs}V_s\right]\nabla T \\ &= \nabla\left[nS_r J_f + (1-n)J_s\right] - nS_r T\left(\frac{\partial P}{\partial T}\right)_{\rho_f}\nabla V_f - (1-n)T\beta\frac{\partial \varepsilon_s}{\partial t}\end{aligned} \tag{25}$$

When it is assumed that Fourier's law is valid for heat conduction, the following equation are given:

$$\begin{aligned}J_f &= -K_{Tf}\nabla T \\ J_s &= -K_{Ts}\nabla T\end{aligned} \tag{26}$$

where K_T is the coefficient of heat conduction.

The term $(\partial P/\partial T)$ in equation (25) can be modified by applying equation (15) and (16) as follows:

$$\left(\frac{\partial P}{\partial T}\right)_{\rho_f} = \left|\frac{\beta_T}{\beta_P}\right|_{\rho_f = cons\tan t} \tag{27}$$

Disregarding the velocity of a solid, equation (25) is rewritten using equation (6), (9), (26) and (27) in the following form:

$$(\rho C_v)_m \frac{\partial T}{\partial t} + nS_r \rho_f C_{vf} V_{fi} T_{,i} - K_{Tm} T_{,ii}$$
$$- nS_r T \frac{\beta_T}{\beta_P} k(\theta) h_{,ii} + \frac{1}{2}(1-n)\beta T \frac{\partial}{\partial t}\left(u_{i,j} + u_{j,i}\right) = 0 \tag{28}$$

where $(\rho C_v)_m$ and K_{Tm} are expressed as follows:

$$(\rho C_v)_m = nS_r \rho_f C_{vf} + (1-n)\rho_s C_{vs} \tag{29}$$

and

$$K_{Tm} = nS_r K_{Tf} + (1-n)K_{Ts} \tag{30}$$

Equation (28) is an energy conservation law in which the effects of stress-deformation and ground water flow are considered. The first, second and third terms at the right-hand side express changes in energy due to heat conduction, pore water pressure and reversible energy caused by solid deformation, respectively.

5) Governing equations

Equation (7), (21) and (28) represent the governing equations for a coupled tharmal, hydraulic and mechanical problem proposed by Ohnish et al. This model was verified with the available analytical and experimental results. These equations are used by means of a total head expression such as,

$$\left[\frac{1}{2} C_{ijkl}\left(u_{k,l} + u_{l,k}\right) - \beta \delta_{ij}(T - T_o) + \chi \delta_{ij} \rho_f g \psi\right]_{,j} + \overline{\rho_s} b_i = 0$$

$$\left\{\rho_f k(\theta)_{ij} h_{,j}\right\}_{,i} - \rho_{fo} nS_r \rho_f g \beta_P \frac{\partial h}{\partial t} - \rho_f \frac{\partial \theta}{\partial \psi}\frac{\partial h}{\partial t} - \rho_f S_r \frac{\partial u_{i,i}}{\partial t} + \rho_{fo} nS_r \beta_T \frac{\partial T}{\partial t} = 0 \tag{31}$$

$$(\rho C_v)_m \frac{\partial T}{\partial t} + nS_r \rho_f C_{vf} V_{fi} T_{,i} - K_{Tm} T_{,ii}$$
$$- nS_r T \frac{\beta_T}{\beta_P} k(\theta) h_{,ii} + \frac{1}{2}(1-n)\beta T \frac{\partial}{\partial t}\left(u_{i,j} + u_{j,i}\right) = 0$$

where $\overline{\rho_s} = (1-n)(\rho_s - S_r \rho_f)$ and ρ_s is the density of a solid phase.

2.3 Governing equations of extended coupled THM model for buffer material

The behaviour of the buffer material is influenced by the interdependence of thermal, hydraulic and mechanical phenomena. To treat the water/vapor movement and heat induced water movement, the continuity equation used in the extended THAMES code is as follows;

$$\left\{\xi\rho_l D_\theta \frac{\partial\theta}{\partial\psi}(h_{,i}-z_{,i})+(1-\xi)\frac{{\rho_l}^2 gK}{\mu_l}h_{,i}\right\}+\{\rho_l D_T T_{,i}\}_{,i}$$
$$-\rho_{lo} nS_r\rho_l g\beta_P\frac{\partial h}{\partial t}-\rho_l\frac{\partial\theta}{\partial\psi}\frac{\partial h}{\partial t}-\rho_l S_r\frac{\partial u_{i,i}}{\partial t}+\rho_{lo} nS_r\beta_T\frac{\partial T}{\partial t}=0 \tag{32}$$

where D_θ is the isothermal water diffusivity, θ is the volumetric water content, ψ is the water potential head and K is the intrinsic permeability. The symbol ξ is the unsaturated parameter so that ξ=0 at the saturated zone, ξ=1 at the unsaturated zone. The symbol μ_l is the viscosity of water, ρ_l is the density of water, g is the gravitational acceleration. D_T is the thermal water diffusivity, n is the porosity, S_r is the degree of saturation, β_P is the compressibility of water, β_T the thermal expansion coefficient of water and z is the elevation head. u_i is the displacement vector, T is temperature, h is the total head and t is time. The subscript 0 means the reference state. This equation means that the water flow in the unsaturated zone is expressed by the diffusion equation and in the saturated zone by the Darcy's law.

The energy conservation equation has to treat the energy change by evaporation. The equation is given as

$$(\rho C_v)_m\frac{\partial T}{\partial t}+nS_r\rho_l C_{vl}V_{li}T_{,i}-K_{Tm}T_{,ii}+L\left\{D_{\theta v}\frac{\partial\theta}{\partial\psi}(h_{,i}-z_{,i})\right\}_{,i}$$
$$+nS_r T\frac{\beta_T}{\beta_P}\left\{\xi D_\theta\frac{\partial\theta}{\partial\psi}(h_{,i}-z_{,i})+(1-\xi)\frac{\rho_l gK}{\mu_l}h_{,i}+D_T T_{,i}\right\}_{,i}$$
$$+\frac{1}{2}(1-n)\beta T\frac{\partial}{\partial t}(u_{i,j}+u_{j,i})\delta_{ij}=0 \tag{33}$$

where $(\rho C_v)_m$ is the specific heat of the material consisting of water and the soil particles, C_{vl} is the specific heat of water, V_{li} is the velocity vector of water, K_{Tm} is the thermal conductivity of consisting of water and the solid particles, L is the latent heat of vaporization per unit volume and $D_{\theta v}$ is the vapor diffusivity.

The equilibrium equation has to take the swelling behavior into account.

$$\left[\frac{1}{2}C_{ijkl}\left(u_{k,l}+u_{l,k}\right)-F\pi\delta_{ij}-\beta\delta_{ij}\left(T-T_o\right)+\chi\delta_{ij}\rho_l g\left(h-z\right)\right]+\rho b_i=0 \tag{34}$$

where C_{ijkl} is the elastic matrix, ρ is the density of the medium and b_i is the body force. χ is the parameter for the effective stress, χ=0 at the unsaturated zone, χ=1 at the saturated zone. The symbol F is the coefficient relating to the swelling pressure process and $\beta = (3\lambda + 2\mu)\ \alpha_s$, where $\lambda$and μ are Lame's constants and α_s is the thermal expansion coefficient.

The swelling pressure πcan be assumed to be the function of water potential head (ψ) as follows;

$$\pi(\theta_1)=\rho_l g(\Delta\psi)=\rho_l g(\psi(\theta_1)-\psi(\theta_0))=\rho_l g\int_{\theta_o}^{\theta_1}\frac{\partial\psi}{\partial\theta}d\theta \tag{35}$$

where θ_0 is the volumetric water content at the initial state. This is based on the theory that swelling pressure is equivalent to the water potential.

2.4 Initial and boundary condition

It is necessary to establish the following initial and boundary conditions in order to solve the governing equations.

Initial conditions:

$$u_i(\tilde{x},t)=\hat{u}_i(\tilde{x},0) \tag{36}$$

$$h(\tilde{x},t)=\hat{h}(\tilde{x},0) \tag{37}$$

$$T(\tilde{x},t)=\hat{T}(\tilde{x},0) \tag{38}$$

Boundary condition:

- displacement; $u_i(\tilde{x},t)=\hat{u}_i(\tilde{x},t)$ (39)

or traction; $$\sigma_{ij}(\tilde{x},t)n_j(\tilde{x}) = \hat{T}_i(\tilde{x},t) \quad (40)$$

• total head; $$h(\tilde{x},t) = \hat{h}(\tilde{x},t) \quad (41)$$

or flow rate; $$\{k(\theta)h_{,i}\}n_i = -\hat{Q}(\tilde{x},t) \quad (42)$$

• temperature; $$T(\tilde{x},t) = \hat{T}(\tilde{x},t) \quad (43)$$

or heat flow; $$K_{Tm}T_{,i}n_i = -\hat{Q}_T(\tilde{x},t) \quad (44)$$

where, $\tilde{x}$ is the position vector, n_j is the unit normal vector, $\hat{u}$ is the known displacement, $\hat{h}$ is the known head, $\hat{T}_i$ is the known surface traction, $\hat{Q}$ is the prescribed flow rate and $\hat{Q}_T$ is the prescribed heat flow.

2.5 Numerical techniques

The Galerkin type finite element technique is employed to formulate a finite element discretization. In order to obtain stable solution, linear isoparametric elements are used to represent the behavior of total head *h* and temperature *T*. Quadratic isoparametric elements are used to express displacement u_i. In order to integrate time derivatives, a time weighting factor is introduced, and thus, any type of finite difference scheme may be applied.

3 Parameters for Analysis

3.1 Parameters of bentonite MX-80

For the simulation of Prototype Repository, SKB carried out many laboratory experiments about the bentonite MX-80. The initial conditions of bentonite MX-80 at the laboratory experiments are as follows.

Dry density: ρ_d = 1.67 g/cm^3

Water content: ω= 0.17

Void ratio: e = 0.77

Degree of saturation: S_r = 0.61

In this chapter, we show the parameters of materials for simulation by THAMES. Almost parameter except for the hydraulic conductivity, thermal vapor flow diffusivity and swelling pressure parameter are the same with those used for the simulation conducted by SKB (Börgesson and Herneilind, 1999).

1) Thermal property

The thermal conductivity λ of MX-80 is obtained as a function of degree of saturation S_r. Figure 1 shows the measurement result. For the simulation, we used the relation as shown in Table 1.

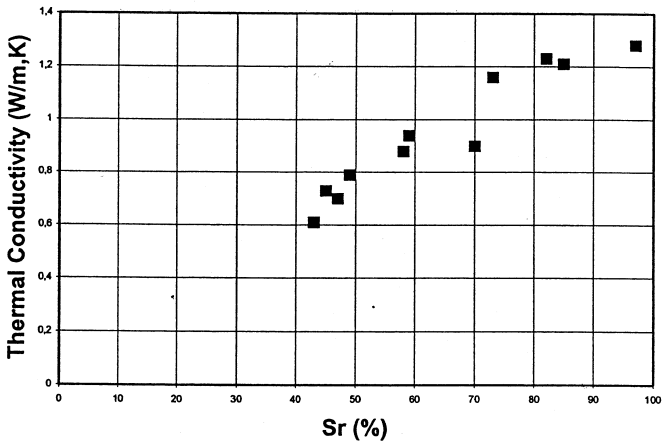

Figure 1 *Thermal conductivity of MX-80*

Table 1 Relationship between thermal conductivity λ and degree of saturation S_r

S_r	λ (W/mK)
0.0	0.3
0.2	0.3
0.3	0.4
0.4	0.55
0.5	0.75
0.6	0.95
0.7	1.1
0.8	1.2
0.9	1.25
1.0	1.3

Specific heat c (kJ/kgK) is a function of water content ω.

$$c = \frac{80.0 + 4.2\omega}{100 + \omega} \tag{45}$$

Table 2 shows the relationship between specific heat and water content calculated from equation (45).

Table 2 Relationship between specific heat and water content

ω(%)	C (J/kgK)
0	0.800
10	1.109
20	1.367
30	1.585
100	2.500

2) Hydraulic property

The hydraulic conductivities (k) of MX-80 are measured with different void ratio (e) under the different temperature (T) conditions. Figure 2 shows the example of measurement results. This figure shows the relationship between the void ratio and the hydraulic conductivity. From these experiment results, SKB used the tabulated data shown in Table 3 for the simulation. In this table, hydraulic conductivity is a function of void ratio and temperature. From this table, the relationship between the hydraulic conductivity and temperature at each void ratio is calculated as shown in Figure 3. From this figure, it is known that hydraulic conductivity increase with temperature increasing. Therefore, we estimated the intrinsic permeability K (m^2) from the hydraulic conductivity k (m/s) by using the equation (46).

$$K = \frac{k\mu}{\rho g} \tag{46}$$

where, μ(Pa s) is the viscosity of water, ρ (kg/m^3) is the density of water and g (m/s^2) is the gravitational acceleration.

Figure 4 shows the relationship between the intrinsic permeability and the temperature at each void ratio. From this figure, it is known that the intrinsic permeability is a function of void ratio. Figure 5 shows relationship between the intrinsic permeability and the void ratio. This relationship is expressed as following equation.

$$K = 1.81 \times 10^{-20} (e)^{4.30} \tag{47}$$

For the simulation by THAMES, equation (47) is used as the intrinsic permeability.

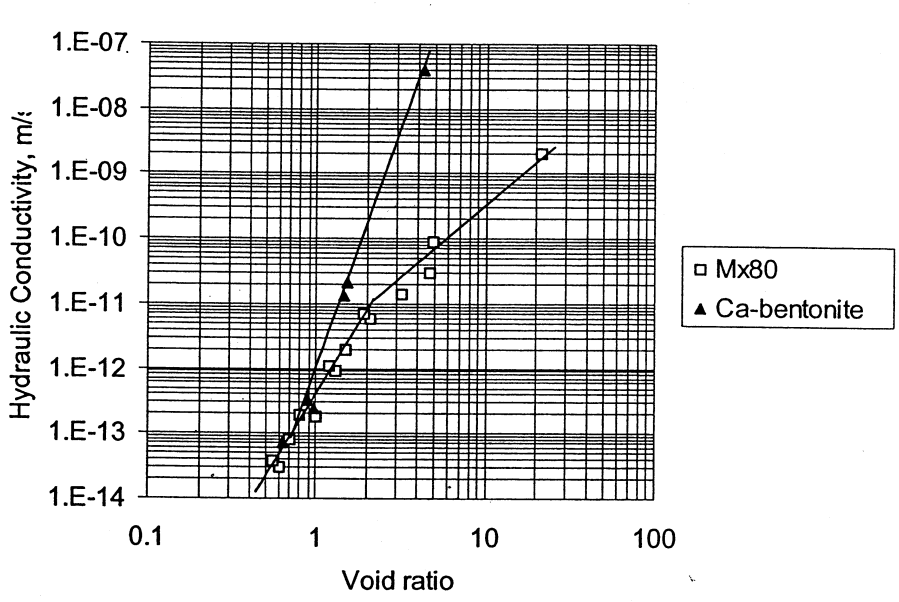

Figure 2 *Measured hydraulic conductivity with different void ratio*

Table 3 Tabulated data of hydraulic conductivity *k* with function of void ratio *e* and temperature *T* for the SKB simulation

T [°C]	*e*	*k* [m/s]
20	0.4	0.035×10^{-13}
20	0.6	0.200×10^{-13}
20	0.8	0.650×10^{-13}
20	1.0	1.750×10^{-13}
40	0.4	0.050×10^{-13}
40	0.6	0.310×10^{-13}
40	0.8	1.000×10^{-13}
40	1.0	2.750×10^{-13}
60	0.4	0.070×10^{-13}
60	0.6	0.440×10^{-13}
60	0.8	1.450×10^{-13}
60	1.0	3.850×10^{-13}
80	0.4	0.100×10^{-13}
80	0.6	0.550×10^{-13}
80	0.8	1.800×10^{-13}
80	1.0	4.900×10^{-13}

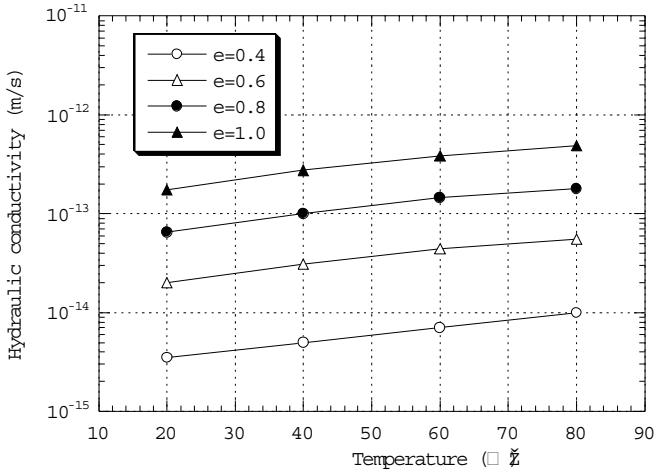

Figure 3 *Temperature dependency of hydraulic conductivity*

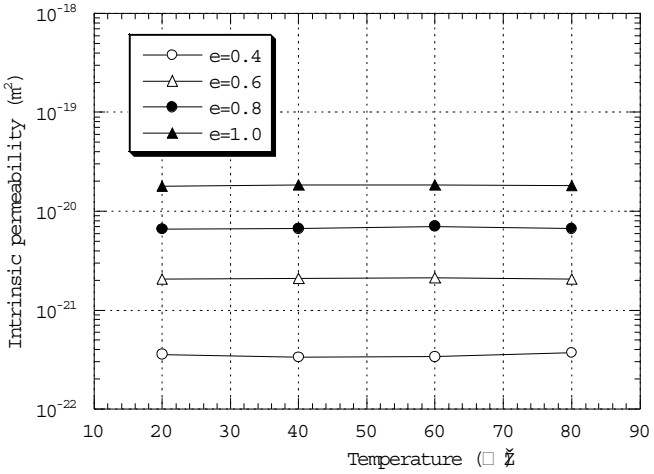

Figure 4 *Temperature dependency of intrinsic conductivity*

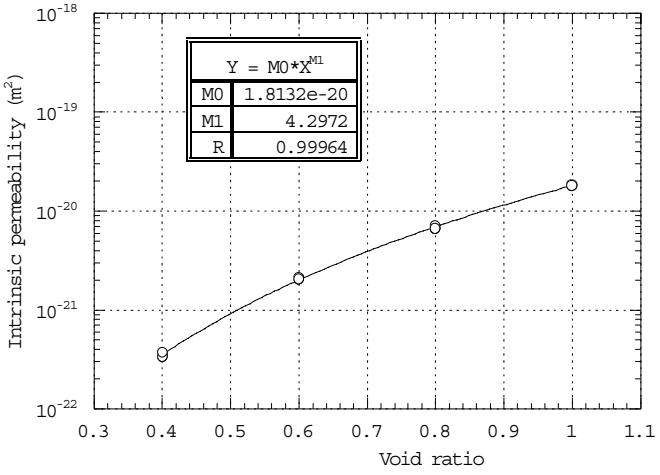

Figure 5 *Relationship between intrinsic permeability and void ratio*

The unsaturated permeability is defined as shown in equation (48) by SKB. In this equation, the unsaturated permeability is a function of the degree of saturation.

$$k_p = (S_r)^{\delta} k \tag{48}$$

where, k_p is the hydraulic conductivity of partly saturated soil, k is the hydraulic conductivity of completely saturated soil and δ is the parameter (usually between 3 and 10).

And the parameter in equation (48) is obtained as follows.

$$\delta = 3 \tag{49}$$

Therefore, the unsaturated permeability when the temperature is 20°C and the void ratio is 0.4 is calculated as shown in Figure 6.

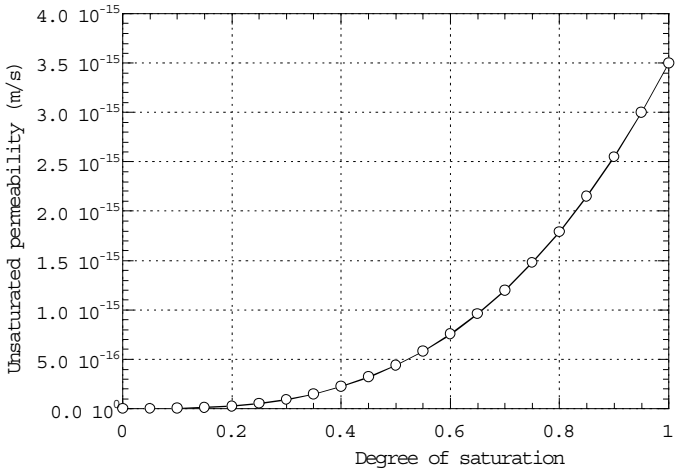

Figure 6 *Unsaturated permeability of MX-80(Temperature 20°C, Void ratio 0.4)*

The water retention curve of MX-80 is shown in Figure 7.

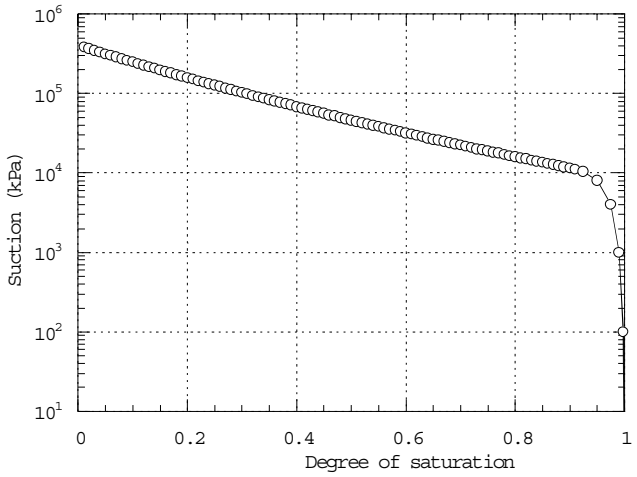

Figure 7 *Water retention curve of MX-80*

The thermal vapor flow diffusivity is determined by temperature gradient test conducted by SKB. Test apparatus is shown in Figure 8. The size of specimen is 50mm in diameter and 50mm in height. The temperature of top and bottom side of specimen was controlled at fixed different temperature. After the several time, specimen was picked up and measured the water content distribution in the specimen.

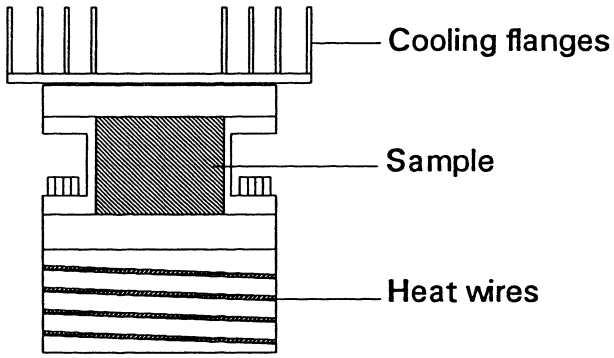

Figure 8 *Test apparatus for temperature gradient test*

SKB used the equation (50), (51) and (52) as the thermal vapor flow diffusivity. In these equations, the thermal vapor flow diffusivity D_{Tv} is a function of the degree of saturation.

$$D_{Tv} = D_{Tvb} \qquad (0.3 \leqq S_r \leqq 0.7) \qquad (50)$$

$$D_{Tv} = D_{Tvb} \cdot \cos^{a}\left(\frac{S_r - 0.7}{0.3} \cdot \frac{\pi}{2}\right) \qquad (0.7 \leqq S_r) \qquad (51)$$

$$D_{Tv} = D_{Tvb} \cdot \sin^{b}\left(\frac{S_r}{0.3} \cdot \frac{\pi}{2}\right) \qquad (S_r \leqq 0.3) \qquad (52)$$

The parameters D_{Tvb}, a and b were determined by back analysis of temperature gradient test. We re-determined the D_{Tvb} by our analysis code THAMES.

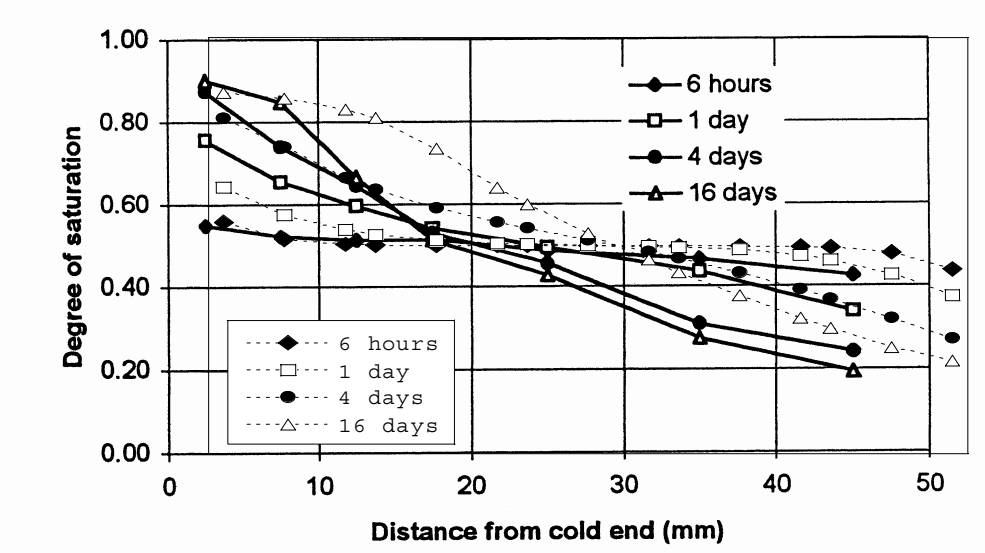

Figure 9 *Comparison of saturation distribution in the specimen between measurement results and simulation results of temperature gradient test (straight line; measurement results, dotted line; simulation results)*

Figure 9 shows the comparison of saturation distribution in the specimen between measurement results and simulation results of temperature gradient test. Initial degree of saturation of the specimen is 50%. The determined values are shown in following equations. Here, the parameter D_{Tvb} is only determined and other parameters a and b are the same with SKB values.

$$D_{Tvb} = 2.0\times10^{-13}\ \mathrm{m^2/sK} \tag{53}$$

$$a = 6 \tag{54}$$

$$b = 6 \tag{55}$$

Figure 10 shows the calculated thermal vapor flow diffusivity as function of the degree of saturation.

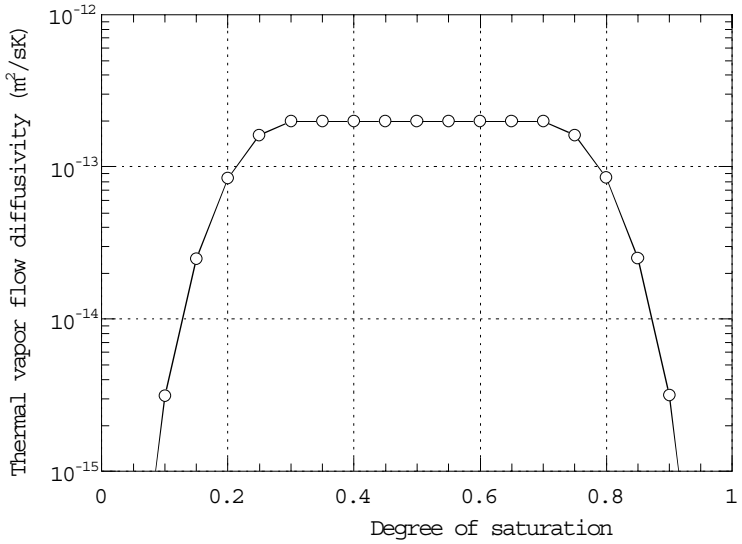

Figure 10 *Thermal vapor flow diffusivity as function of degree of saturation*

3) Swelling property

The parameter for swelling pressure (F in equation (34)) is determined by back analysis of swelling pressure test conducted by SKB. Initial condition is specimen is follows.

Size: diameter 50mm, height 50mm

Degree of saturation: 0.4

Time history of calculated swelling pressure is shown in Figure 11. The parameter F is determined as 0.180.

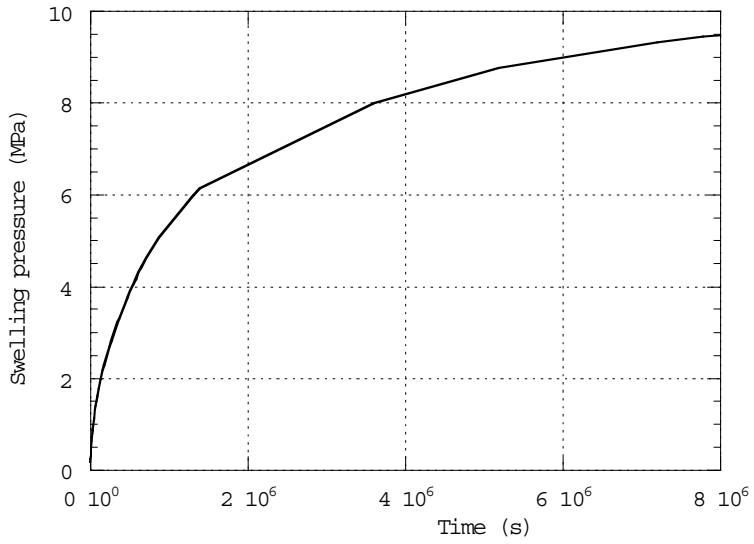

Figure 11 *Calculated swelling pressure*

3.2 Parameters of backfilling material

In the Prototype Repository Project, mixed material with bentonite and crushed rock (B:S=3:7) will be used for the backfilling of drift. Backfilling material is compacted in situ and dry density is 1.75g/cm^3 (void ratio 0.57, saturated water content 20.7%).

Parameters of backfilling material for the simulation are as follows.

1) Thermal property

The thermal properties of backfilling material are constant as following values.

Thermal conductivity: λ=1.5W/mK (56)

Specific heat: c=1.2kJ/kgK (57)

2) Hydraulic property

Hydraulic conductivity k of backfilling material is as follow.

Hydraulic conductivity: k=2.0E-10m/s (58)

The relationship between the suction and the degree of saturation for the simulation is shown in Table 4. Figure 12 shows the water retention curve of the backfilling material. The unsaturated permeability is calculated by equation (48) and (49).

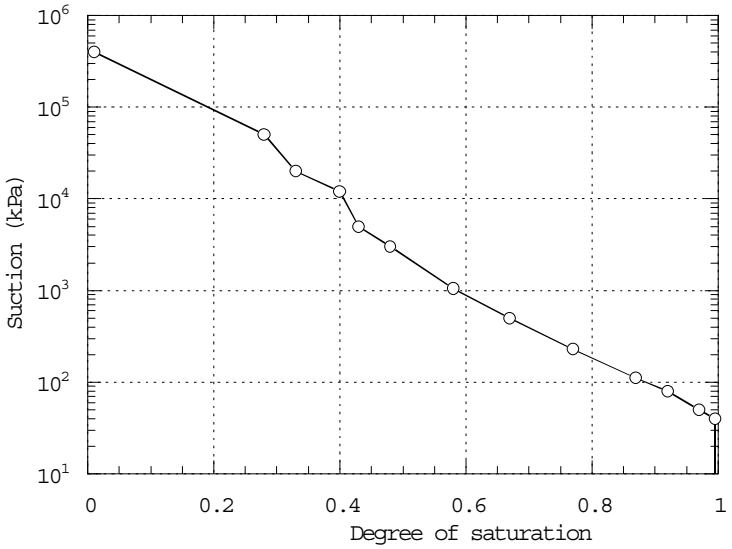

Figure 12 *Water retention curve of backfilling material*

Table 4 Relationship between the suction and the degree of saturation of backfilling material

Degree of saturation *Sr* (-)	Suction *Sw* (kPa)
0.01	400000
0.28	50000
0.33	20000
0.40	12000
0.43	5000
0.48	3000
0.58	1050
0.67	500
0.77	230
0.87	110
0.92	80
0.97	50
0.995	40
1.0	0

3) Mechanical property

The Young's modulus and the poison's ratio of backfilling material for the simulation are as follows.

Young's modulus: E=30MPa (59)

Poison's ratio: ν=0.3 (60)

3.3 Parameters of surrounding rock

1) Thermal property

The thermal properties of surrounding rock are constant as following values.

Thermal conductivity: λ=3.0W/mK (61)

Specific heat: c=0.8kJ/kgK (62)

2) Hydraulic property

Hydraulic conductivity of surrounding rock for the simulation is constant. However, because the hydraulic property of real rock is heterogeneous, some values are used for the simulation and the effect of permeability of rock on the simulation is examined.

Hydraulic conductivity: k=10^{-10} to 10^{-14}m/s (63)

The relationship between the suction and the degree of saturation for the simulation is shown in Table 5. Figure 13 shows the water retention curve of the surrounding rock. The unsaturated permeability is calculated by equation (48) and (49).

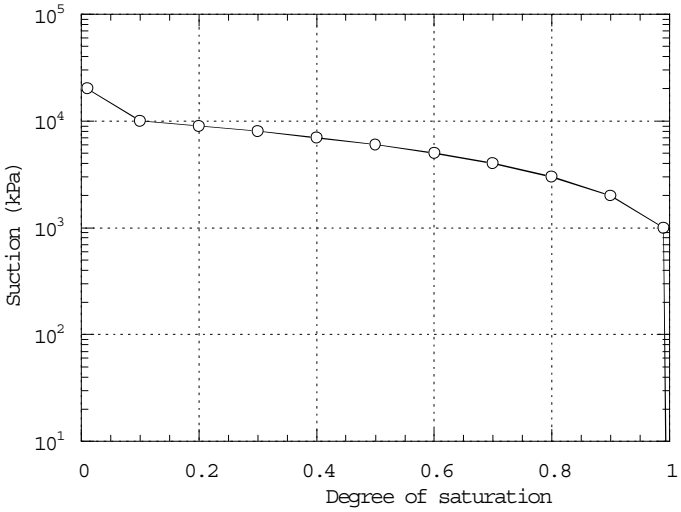

Figure 13 *Water retention curve of surrounding rock*

Table 5 Relationship between the suction and the degree of saturation of surrounding rock

Degree of saturation *Sr* (-)	Suction *Sw* (kPa)
0.01	20000
0.1	10000
0.2	9000
0.3	8000
0.4	7000
0.5	6000
0.6	5000
0.7	4000
0.8	3000
0.9	2000
0.99	1000
1.0	0

3) Mechanical property

The Young's modulus, the poison's ratio and the density of surrounding rock for the simulation are as follows.

Young's modulus: E=1,850MPa (64)

Poison's ratio: ν=0.3 (65)

Density: ρ=2.6g/cm^3 (66)

3.4 Parameters of heater

Parameters of the heater for the simulation are as follows.

Thermal property: λ=200W/mK (67)

Specific heat: c=0.4kJ/kgK (68)

Young's modulus: E=210,000MPa (69)

Poison's ratio: ν=0.3 (70)

Density: ρ=7.0g/cm^3 (71)

4 Analysis of prototype repository

4.1 Analysis model

Analysis is carried out by two-dimensional model. Figure 14 shows the model geometry. Figure 14 (a) is a whole geometry and (b) is geometry of engineering barrier. Analysis region is 11m in width and 74m in height. Figure 15 shows the finite element mesh for the simulation.

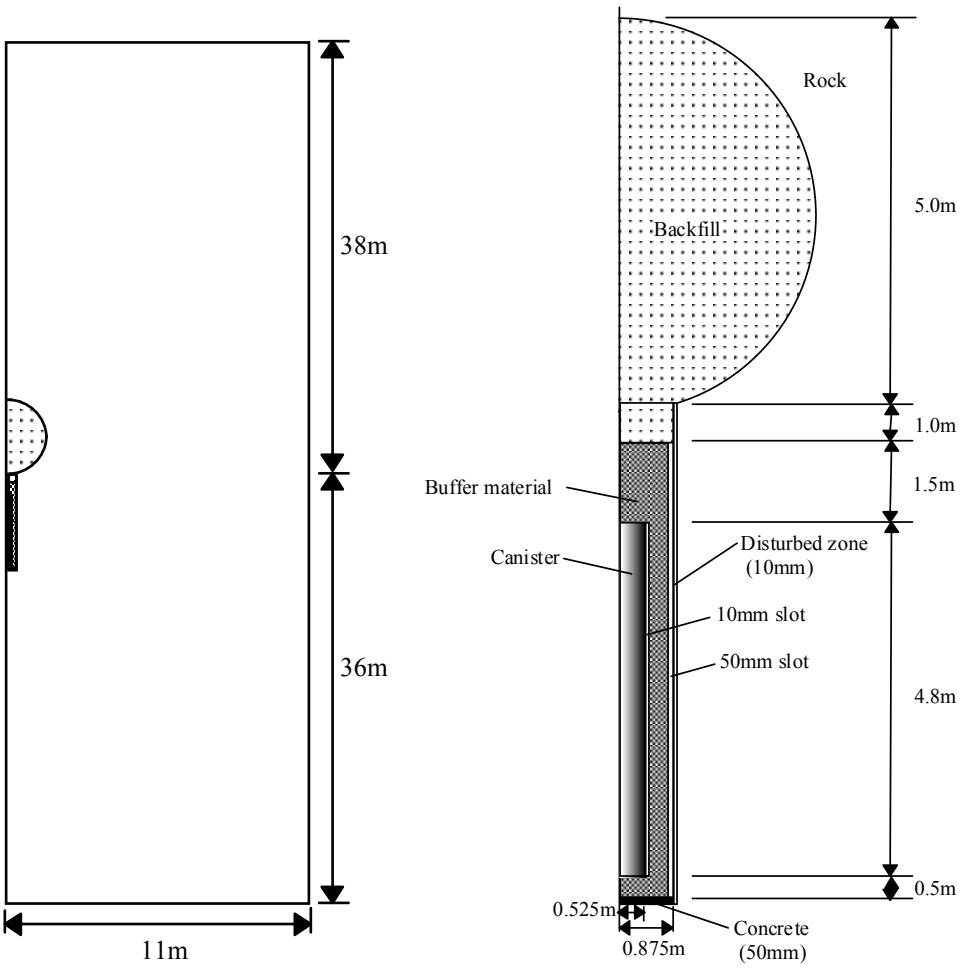

(a) Whole geometry (b) Geometry of engineering barrier

Figure 14 *Model geometry*

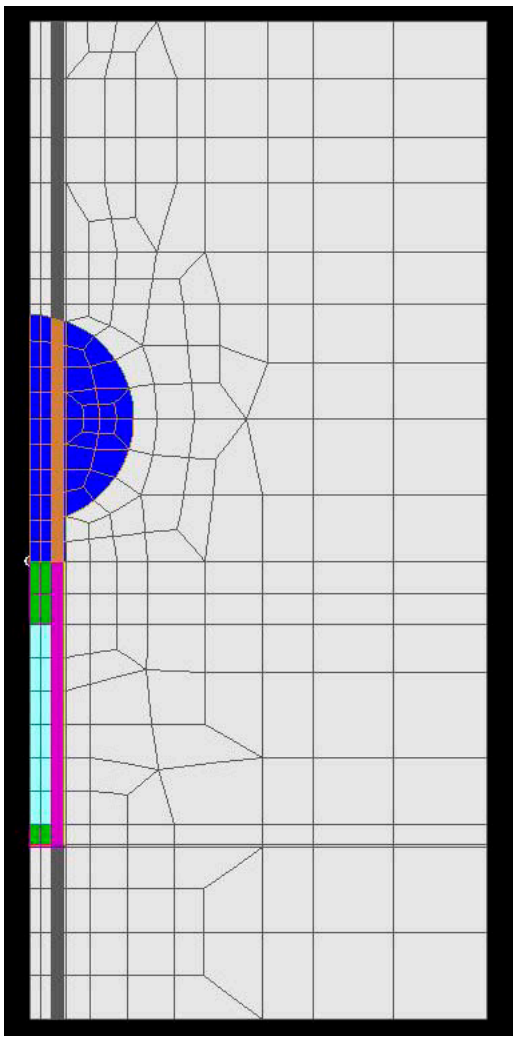

Figure 15 *Finite element mesh*

4.2 Analysis condition

Initial conditions and boundary conditions for the simulation are shown in Figure 16.

(Initial condition)
Water head of surrounding rock: 400m
Degree of saturation of buffer material: 60%
Degree of saturation of backfilling material: 60%
Temperature: 20°C

(Boundary condition)
Hydraulic: upper; constant, other; no flow
Thermal: upper and bottom; constant, other; adiabatic
Mechanical: fixed to the normal direction
Heater: temperature constant (90°C) or heat flux constant (1,800W)

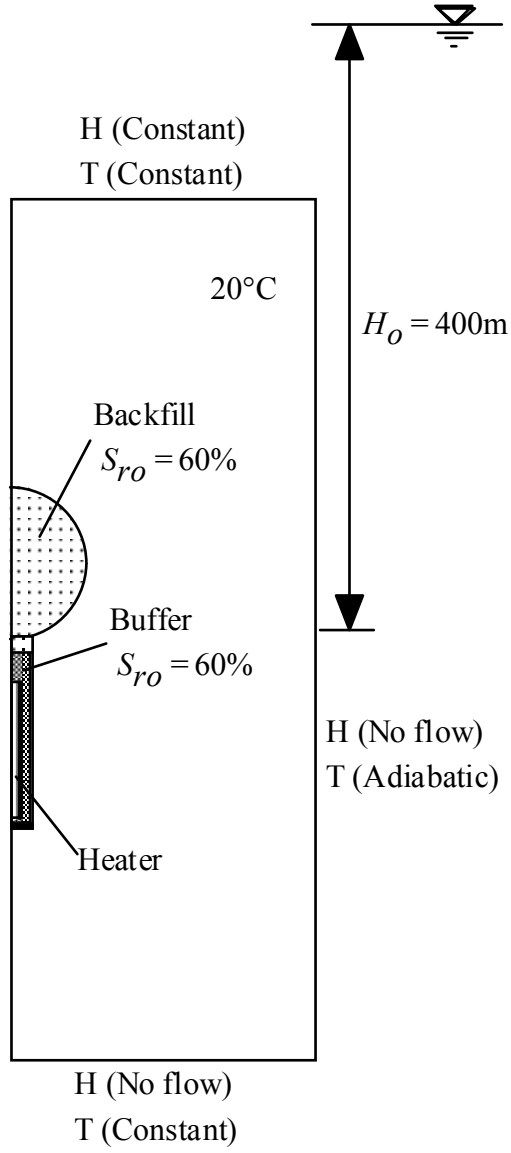

Figure 16 *Initial and boundary conditions*

4.3 Analysis case

Table 6 shows the analysis case. Case0-1 and Case0-2 are the case to research the difference between the boundary condition of heater. Case0-1 is temperature constant condition and Case0-2 is heat flux constant condition. Here, the initial void ratio of buffer material is 0.77 and it is not considered the gap between the heater and the buffer and between the rock and the buffer. This void ratio value of buffer material corresponds to that after saturation. The hydraulic conductivity of rock mass is 10^{-10}m/s. Case1-1, Case1-2 and Case1-3 are the case to research the effect by difference of permeability of rock mass. The hydraulic conductivity of rock mass are 10^{-10}m/s, 10^{-12}m/s, 10^{-14}m/s, respectively. The initial void ratio of buffer material is 0.64. This value corresponds to bentonite block before installation to the test pit. In these cases, it is not considered the gap between the heater and the buffer and between the rock and the buffer. Because the bentonite of Case1-1 corresponds to that before the installation and bentonite of Case0-1 corresponds to that after saturation (after swelling), real

phenomena will be occurred between these two cases. Above simulations are carried out by TH analysis. The reasons are that structure change in the bentonite due to the swelling is not clear and these simulations focus the effect by the external factor, e.g., boundary condition of heater and permeability of rock mass. Case2-1 is a case that it is considered the gap between the heater and the buffer and between the rock and the buffer. The thermal property of gap is the same with water. This simulation is carried out by THM analysis because the closing of gap must be considered. Furthermore, we carried out the comparison between the TH analysis and THM analysis when the gap is not considered in the model by Case 0-1 and Case1-1. Case3-1, Case3-2 and Case3-3 are the case to research the effect by difference of thermal vapor flow diffusivity of bentonite. The thermal vapor flow diffusivity of bentonite are $4 \cdot 10^{-13} m^2/sK$, $6 \cdot 10^{-13} m^2/sK$, $10 \cdot 10^{-13} m^2/sK$, respectively. These values are two, three and five times of determined value from the laboratory test shown in section 3.1.

Regarding the parameter of the buffer, only hydraulic conductivity (intrinsic permeability) is a function of void ratio (see equation (47)). Therefore, in case of THM analysis only hydraulic conductivity changes with the change of void ratio, other input parameter is not function of void ratio.

Table 6 Analysis case

Case	Boundary condition of heater	Initial void ratio of buffer material	Hydraulic conductivity of rock mass (m/s)	Consideration of gap	Thermal vapor flow diffusivity (m^2/sK)	Analysis
Case0-1	Temperature constant	0.77	10^{-10}	No	$2.0 \cdot 10^{-13}$	TH and THM
Case0-2	Heat flux constant	0.77	10^{-10}	No	$2.0 \cdot 10^{-13}$	TH
Case1-1	Temperature constant	0.64	10^{-10}	No	$2.0 \cdot 10^{-13}$	TH and THM
Case1-2	Temperature constant	0.64	10^{-12}	No	$2.0 \cdot 10^{-13}$	TH
Case1-3	Temperature constant	0.64	10^{-14}	No	$2.0 \cdot 10^{-13}$	TH
Case2-1	Temperature constant	0.64	10^{-10}	Yes	$2.0 \cdot 10^{-13}$	THM
Case3-1	Temperature constant	0.64	10^{-10}	No	$4.0 \cdot 10^{-13}$	TH
Case3-2	Temperature constant	0.64	10^{-10}	No	$6.0 \cdot 10^{-13}$	TH
Case3-3	Temperature constant	0.64	10^{-10}	No	$10.0 \cdot 10^{-13}$	TH

4.4 Analysis results

At first, we carried out the analyses of Case0-1 and Case0-2 and compared the difference due to the boundary conditions of heater. As a result, we could not obtain good result in the Case0-2. This will be because the heat flux of heater was too high in that simulation. Figure 17 shows the time history of degree of saturation in the buffer at the center level of heater (along the output line as shown in the figure at right). The degree of saturation near the heater became low due to temperature gradient and it showed the minimum value (approximately 40%) after about 300 days from the start of heating. After that the degree of saturation increased gradually as a whole in the buffer and the buffer became saturation after about 6,000 days from the star of heating. Figure 18 shows the time history of temperature along the output line in the right figure. It is known that temperature did not become constant after the saturation of the buffer. Temperature became constant after 10,000 days from the star of heating.
Figure 19 shows the time history of degree of saturation in the buffer for Case1-1. Decreasing rate of saturation near the heater in the buffer in this case was larger than that in Case0-1 and minimum value of the degree of saturation was approximately 30%. Furthermore, it needed more time to reach the saturation in the buffer compared with Case0-1. Re-saturation time was approximately 20,000 days. Figure 20 shows the time history of temperature along the output line in the right figure. It is not seen the large difference between Case0-1 and Case1-1. As compared with Case0-1, the speed of temperature increasing for Case1-1 was a little slow because the degree of saturation in the buffer for Case1-1 was lower than Case0-1 but final temperature distribution for Case1-1 was the almost same with Case0-1.
Figure 21 shows the time history of degree of saturation in the buffer for Case1-3. There was no difference between Case1-1 and Case1-3. Figure 22 shows the time history of temperature along the output line in the right figure. There was also no difference. Therefore, it is concluded that re-saturation phenomena in the buffer are not dependent on the permeability of rock mass if the hydraulic conductivity of rock mass is in the 10^{-10} to 10^{-14}m/s range.

Figure 23 shows the time history of degree of saturation in the buffer for Case2-1. As compared with Case1-1, degree of saturation increasing near rock mass in the buffer was faster but the re-saturation time in whole buffer was the almost same with Case1-1. Figure 24 shows the time history of temperature for Case2-1. There was not seen large difference with Case1-1.

Figure 25 to Figure 30 show the simulation results with different thermal vapor flow diffusivity. The degree of decreasing of saturation in the buffer is great with increasing of thermal vapor flow diffusivity. The effect of thermal vapor flow diffusivity is great and it is said that it is important to evaluate the thermal vapor flow diffusivity exactly to estimate the re-saturation phenomena in the buffer precisely.

Figure 31 to 37 show the distribution of degree of saturation and temperature around the disposal tunnel after 30 days, 1 year and 5 years of Case0-1, Case1-1, Case1-2, Case2-1, Case3-1 and case3-3, respectively. After 30 days, degree of saturation of rock mass around the disposal tunnel decreases slightly, however, it recovers to 100% after 1 year. Furthermore, it is known that the effect of permeability of rock mass on the decreasing of saturation of rock mass is little if the permeability of rock mass is in the range between 10^{-10}m/s and 10^{-14}m/s. It is also indicated from these figures that the thermal vapor flow diffusivity of buffer exerts the most influence upon the distribution of degree of saturation and temperature in and around the engineered barrier.

Figure 38 shows the time history of degree of saturation in the buffer with different permeability of rock mass. Black legend is the results of outer side of buffer (near rock mass) and white one is results of inner side of buffer (near heater). Figure 39 shows the time history of temperature at the same points with Figure 38. It is also indicated from these figures that the effect of permeability of rock mass upon the distribution of saturation and temperature in the buffer is small. Figure 40 and Figure 41 show the results with different thermal vapor flow diffusivity. Figure 40 shows the time history of degree of saturation and Figure 41 shows the time history of temperature. As compared with Figure 38, it is much different between each case in Figure 40 because of different thermal vapor flow diffusivity. The degree of decreasing of saturation in the buffer is great with increasing of thermal vapor flow diffusivity. Figure 41 shows the time history of temperature with different thermal vapor flow diffusivity. Because the degree of saturation in the buffer decreases with increasing of thermal vapor flow diffusivity, temperature at the outer side of model decreases because of decreasing of thermal conductivity of buffer. In this simulation, the boundary condition of heater is temperature constant. Therefore, the maximum temperature in the buffer becomes low as the thermal vapor flow diffusivity of buffer is high as shown in Figure 41. However, real waste is heat flux constant rather than temperature constant. At that situation, the maximum temperature in the buffer maybe increases with increasing of thermal vapor flow diffusivity.

Figure 42 to 45 show the comparison of degree of saturation and temperature between the TH analysis and THM analysis. Figure 42 and Figure 43 are the results of Case0-1 and Figure 44 and 45 are the results of Case1-1. In these figure, we carried out the comparison by the effect of coupling when we did not consider the gap in the model. From the Figure 42 and Figure 44, it is known that the increasing speed of degree of saturation near rock mass by THM analysis is earlier than that by TH analysis. This is because of increasing of void ratio due to swelling and it caused the increasing of hydraulic conductivity. On the contrary, the void ratio of buffer near the heater decreases by compression due to the swelling of bentonite near the rock mass, and then the hydraulic conductivity of bentonite near the heater decrease. By the decreasing of hydraulic conductivity of bentonite near the heater, the re-saturation time by the THM analysis is longer than that by the TH analysis. And maximum temperature in the buffer by the THM analysis is lower than that by the TH analysis. In these analyses, the structure change due to the swelling is not considered. In these analyses, pressure due to swelling is only considered. Then void at the swollen part becomes to be expanded by the tension stress of swelling. However, it is considered that the void in the bentonite is filled by the swollen montmorillonite minerals (Pusch 1980a, 1980b, Kimine and Ogata, 1994) and the properties will be changed by the change of void during the water uptaking.

Figure 46 to 49 show the time history of degree of saturation in the buffer and time history of temperature with different model for gap between buffer and rock mass. Figure 46 and Figure 47 are the comparison between TH analysis of Case0-1, Case1-1 and THM analysis of Case2-1. Figure 48 and Figure 49 are the comparison between THM analysis of Case0-1, Case1-1 and THM analysis of Case2-1. At the inner part of buffer that will need the most time to reach the saturation, the re-saturation time of Case2-1 is closed to the results of Case1-1 compared with that of Case0-1. In the Figure 46, re-saturation time by Case1-1 is longer than that of Case2-1, but it will be considered that re-saturation time by TH analysis is shorter than that by THM analysis as shown in Figure 42 and Figure 44. Re-saturation time by THM analysis of Case1-1 is the almost same with that by THM analysis of Case2-1. Therefore, it is concluded that when gap is not considered in the model it is better to use the property at the high density of bentonite before installing into the disposal pit. However, these are the results when we did not consider the structure change inside the bentonite due to the swelling in detail. In order to achieve the more detail evaluation, it needs to consider the structure change inside the bentonite and the parameter change during the swelling.

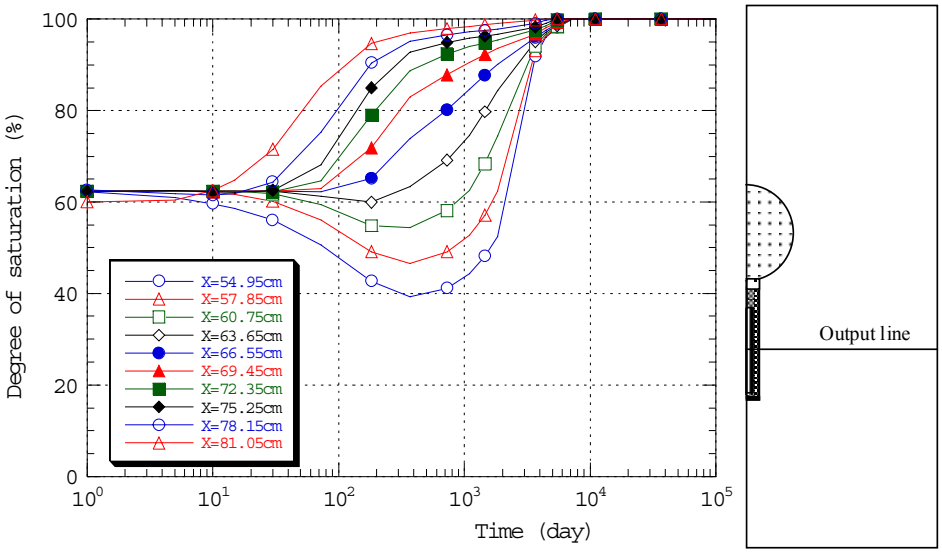

Figure 17 *Time history of degree of saturation in buffer (Case0-1)*

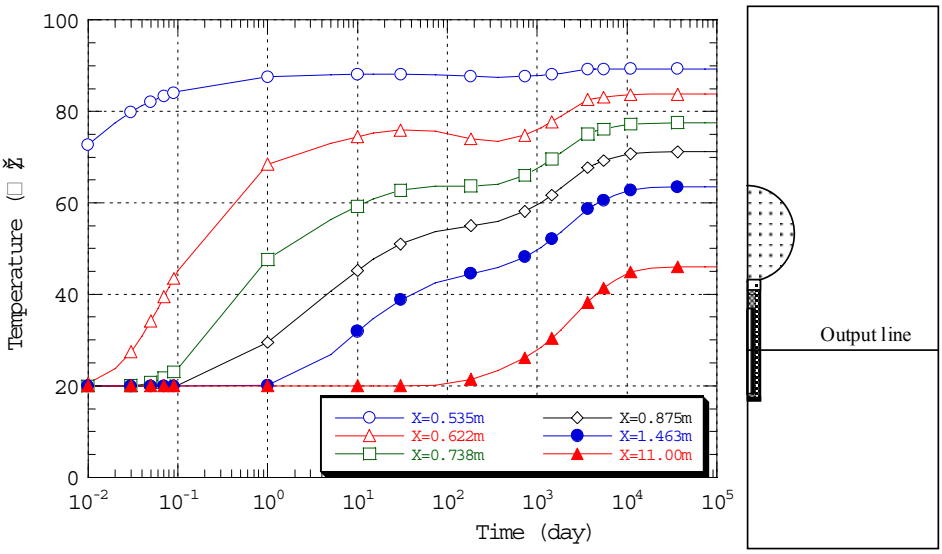

Figure 18 *Time history of temperature in buffer and rock (Case0-1)*

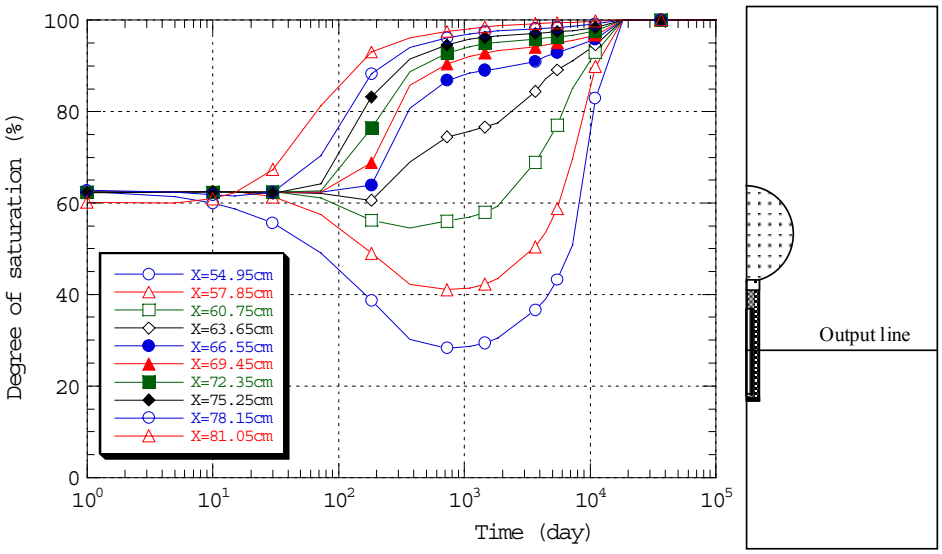

Figure 19 *Time history of degree of saturation in buffer (Case1-1)*

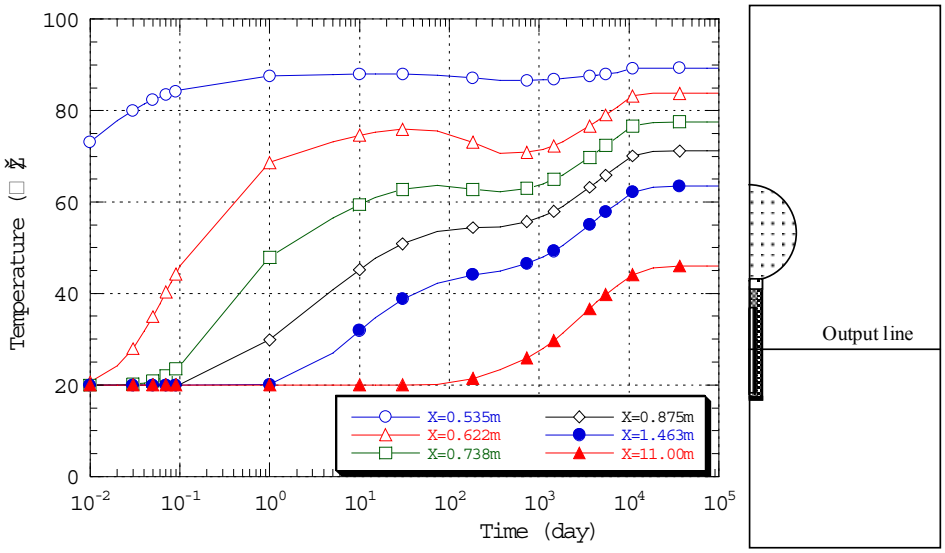

Figure 20 *Time history of temperature in buffer and rock (Case1-1)*

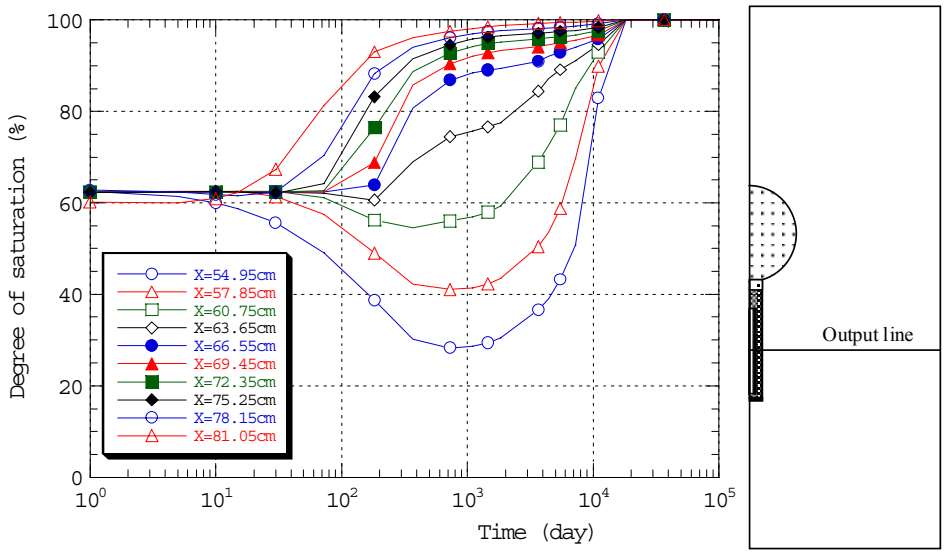

Figure 21 *Time history of water content in buffer (Case1-3)*

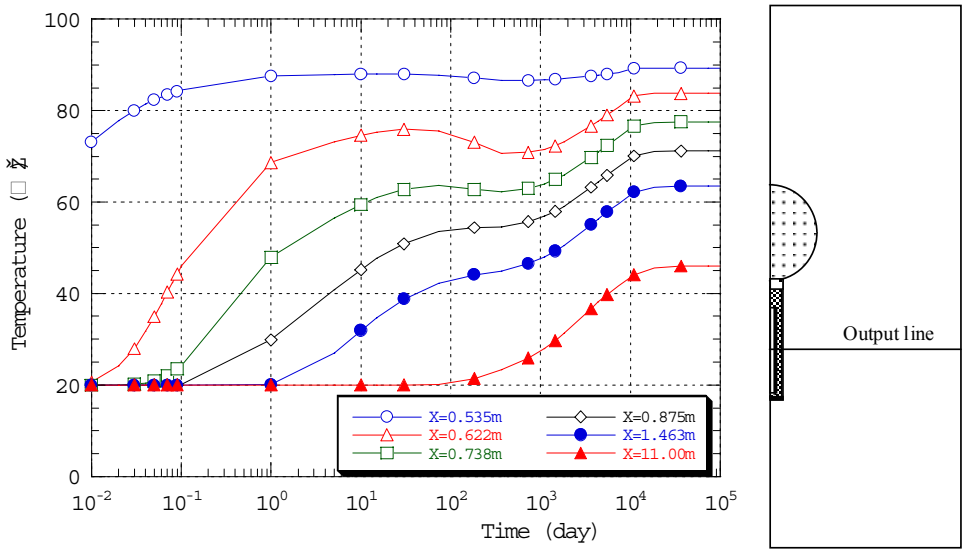

Figure 22 *Time history of temperature in buffer and rock (Case1-3)*

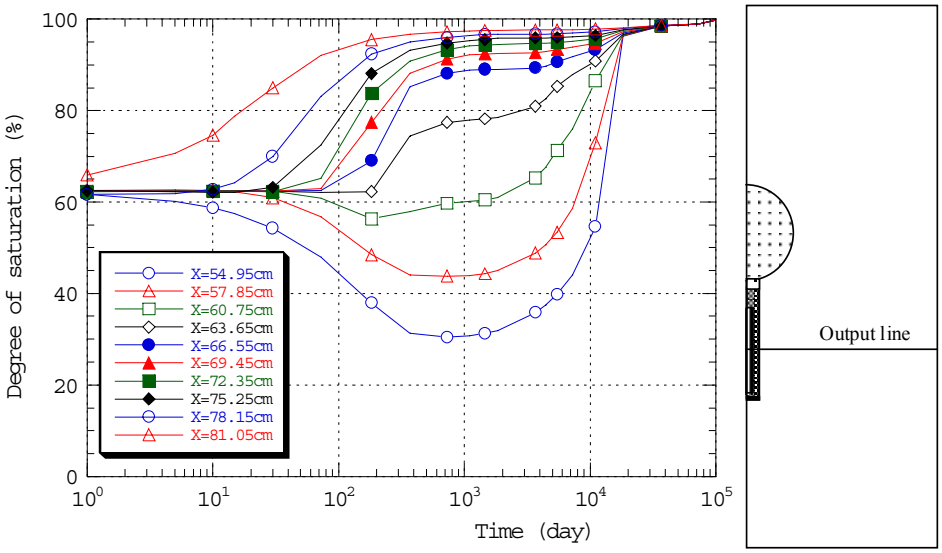

Figure 23 *Time history of degree of saturation in buffer (Case2-1)*

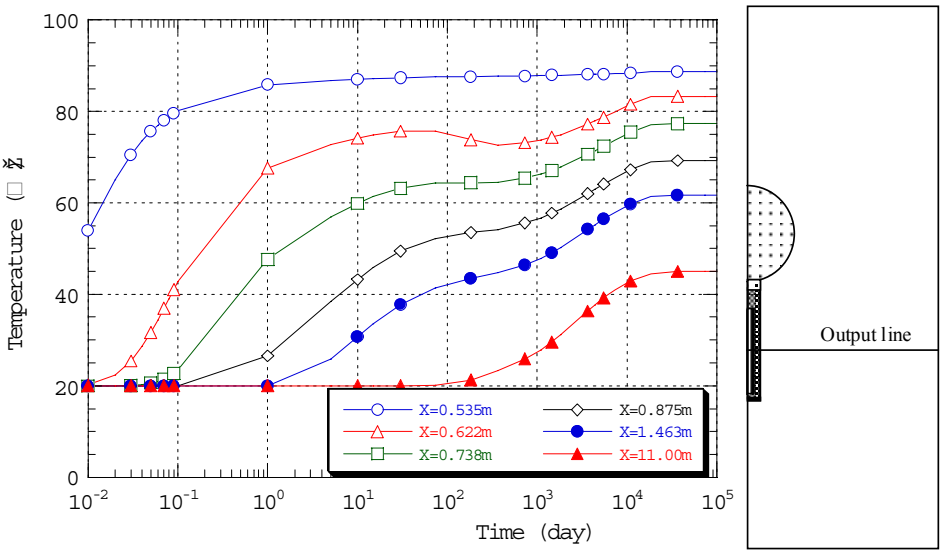

Figure 24 *Time history of temperature in buffer and rock (Case2-1)*

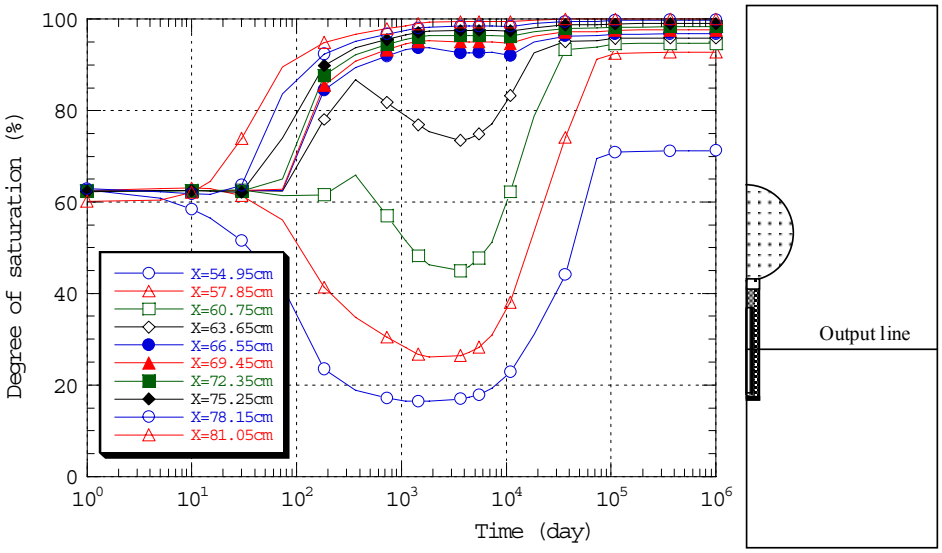

Figure 25 *Time history of degree of saturation in buffer (Case3-1)*

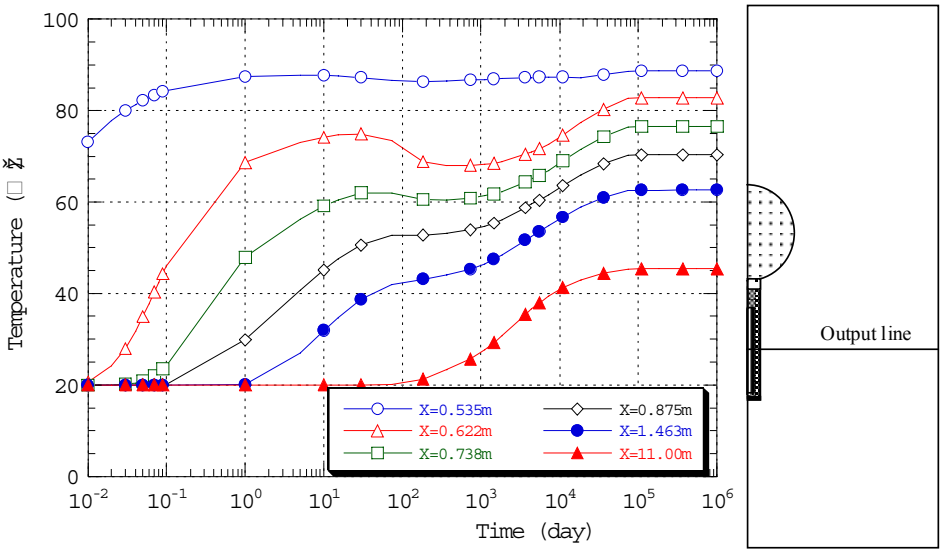

Figure 26 *Time history of temperature in buffer and rock (Case3-1)*

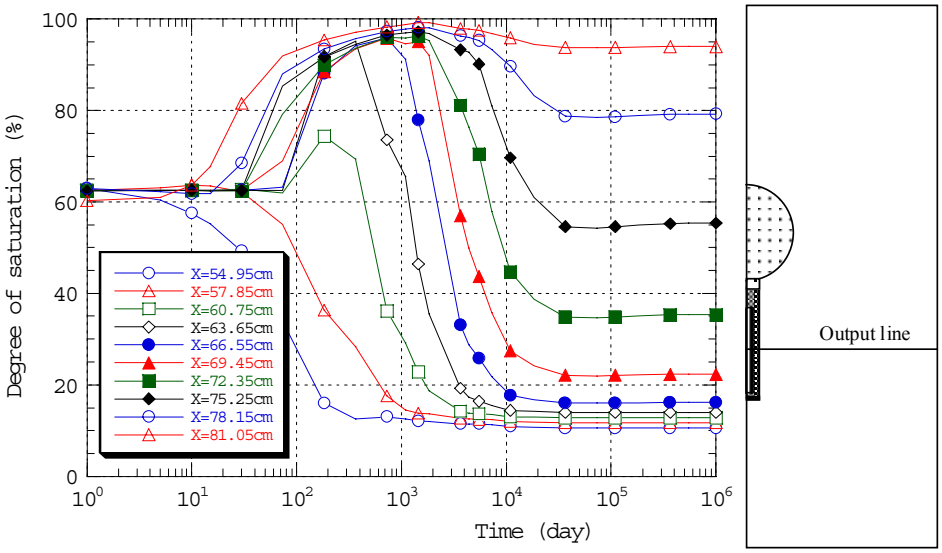

Figure 27 *Time history of degree of saturation in buffer (Case3-2)*

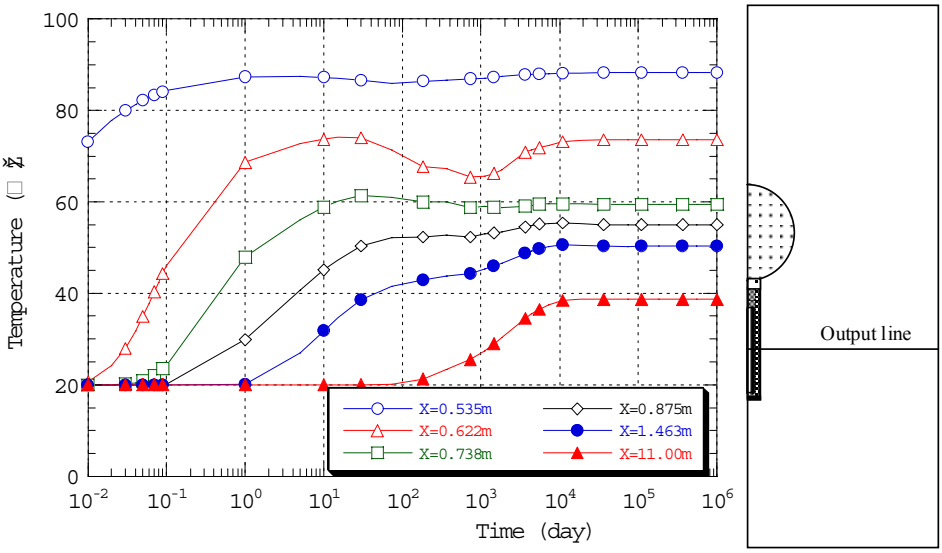

Figure 28 *Time history of temperature in buffer and rock (Case3-2)*

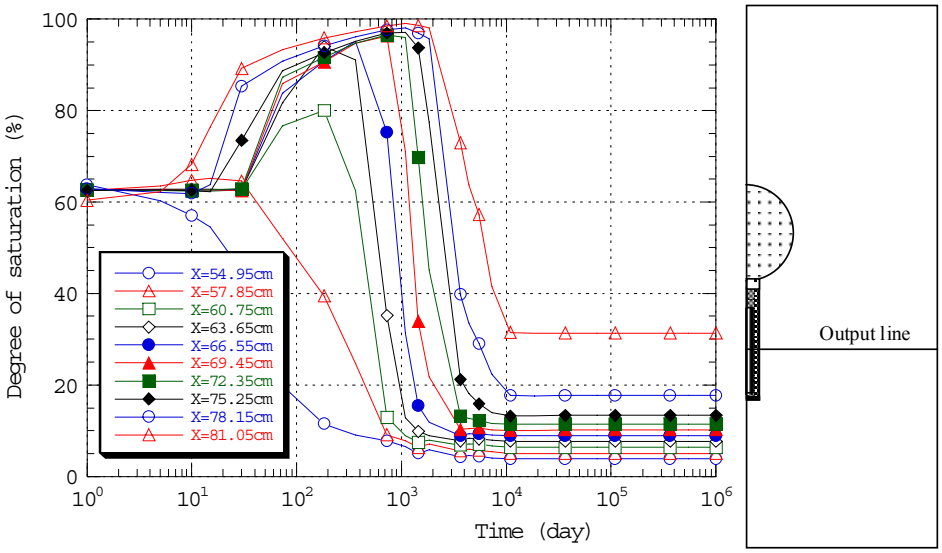

Figure 29 *Time history of degree of saturation in buffer (Case3-3)*

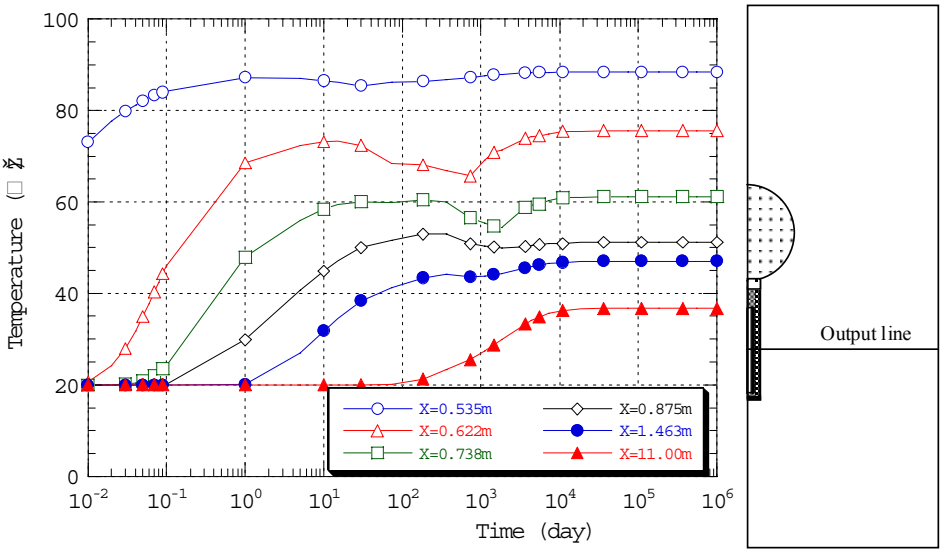

Figure 30 *Time history of temperature in buffer and rock (Case3-3)*

Case0-1	Degree of saturation [%]	Temperature [°C]
After 30 days	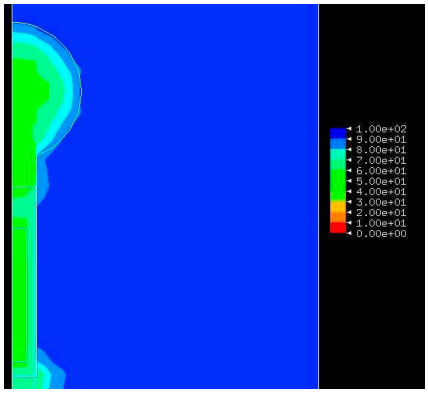	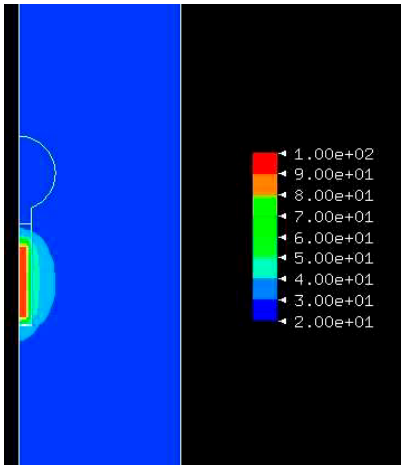
After 1 year	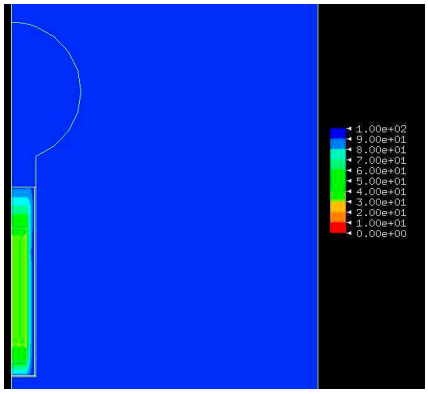	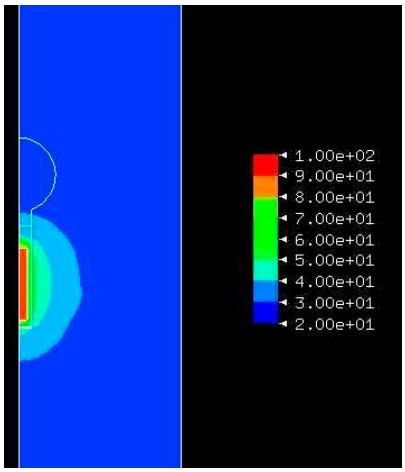
After 5 years	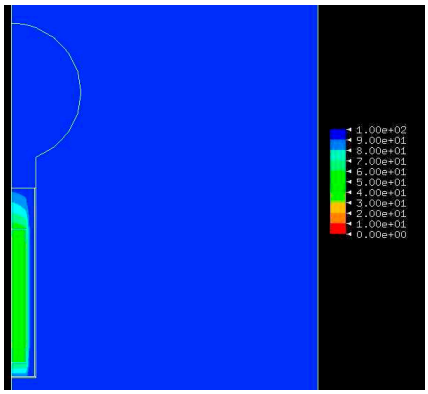	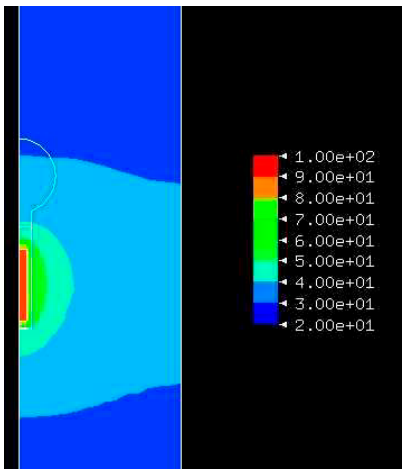

Figure 31 *Distribution of degree of saturation and temperature in buffer and rock (Case0-1)*

Case1-1	Degree of saturation [%]	Temperature [ºC]
After 30 days	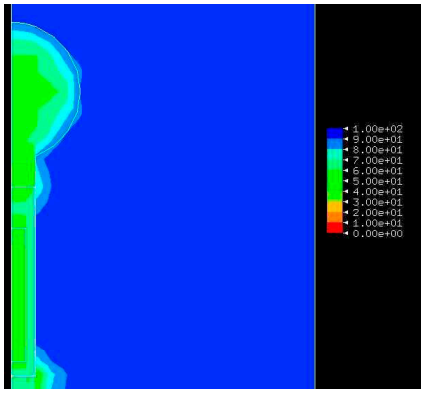	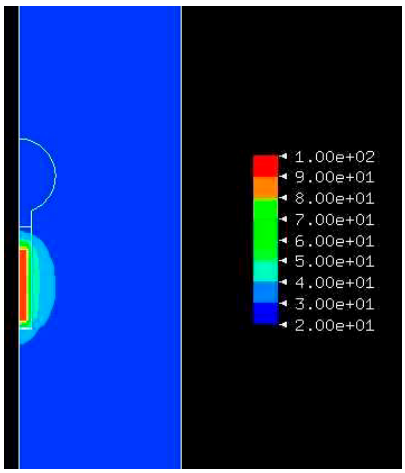
After 1 year	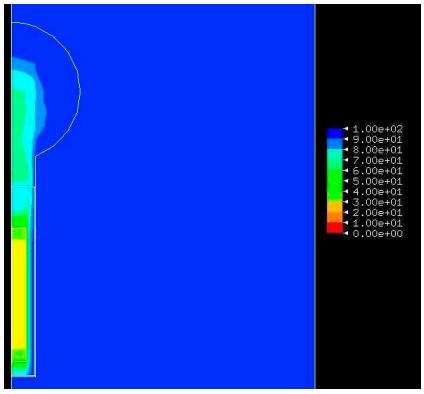	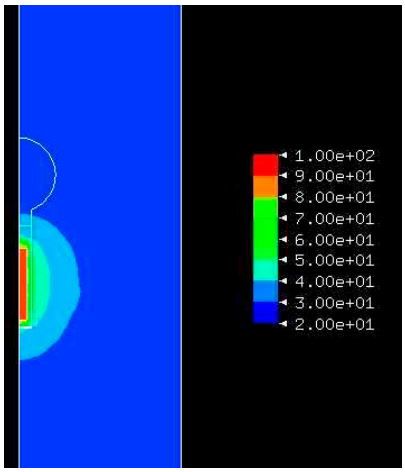
After 5 years	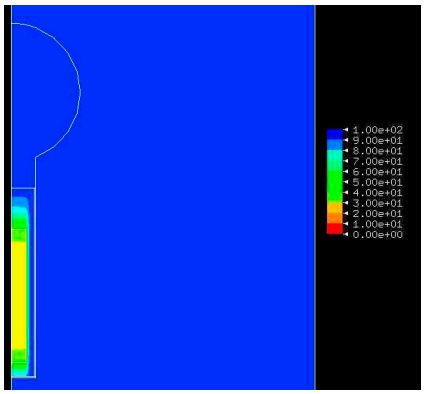	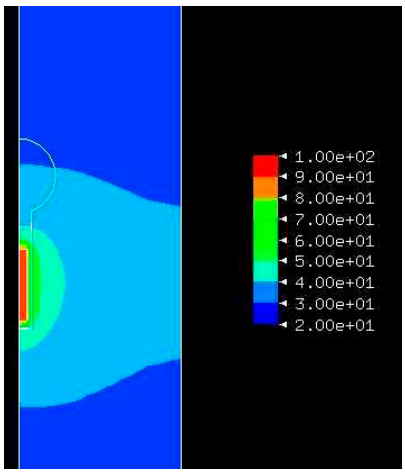

Figure 32 *Distribution of degree of saturation and temperature in buffer and rock (Case1-1)*

Case1-2	Degree of saturation [%]	Temperature [ºC]
After 30 days	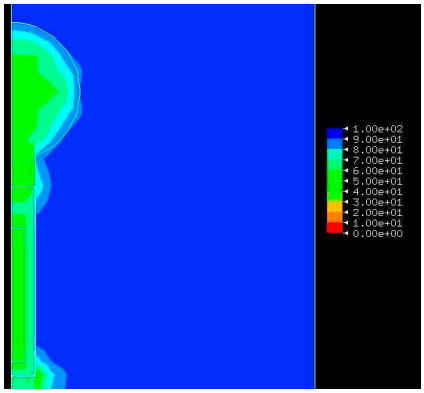	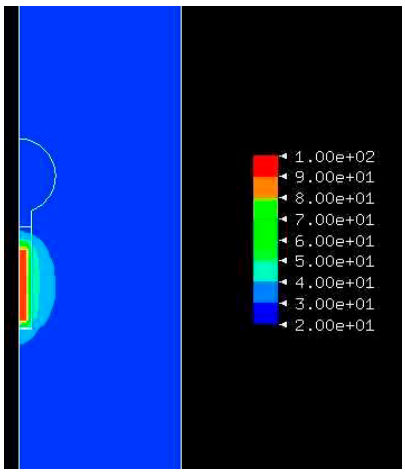
After 1 year	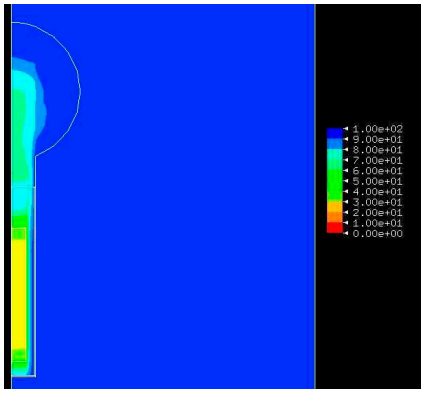	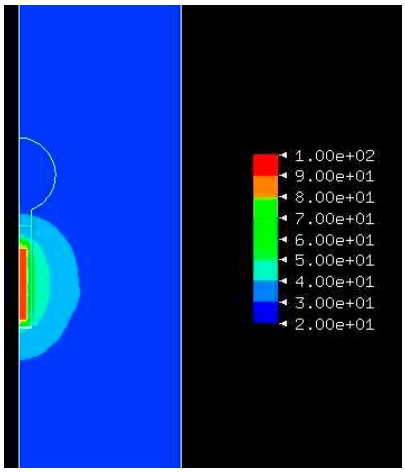
After 5 years	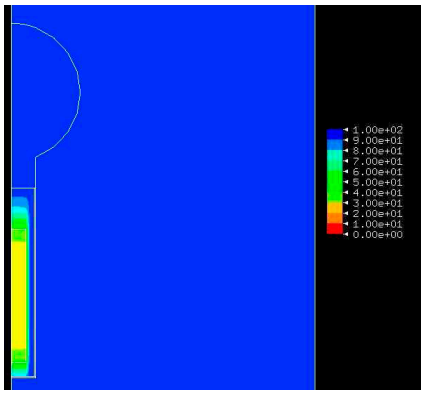	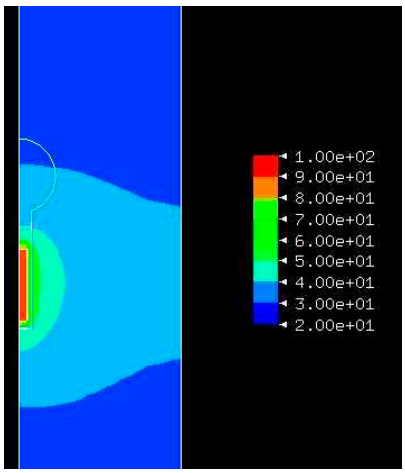

Figure 33 *Distribution of degree of saturation and temperature in buffer and rock (Case1-2)*

Case1-3	Degree of saturation [%]	Temperature [°C]
After 30 days	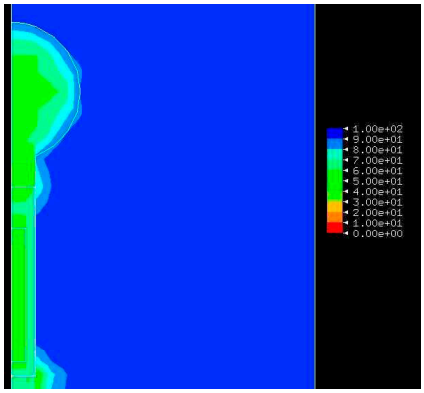	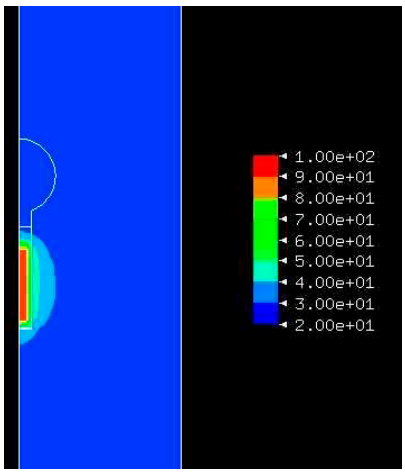
After 1 year	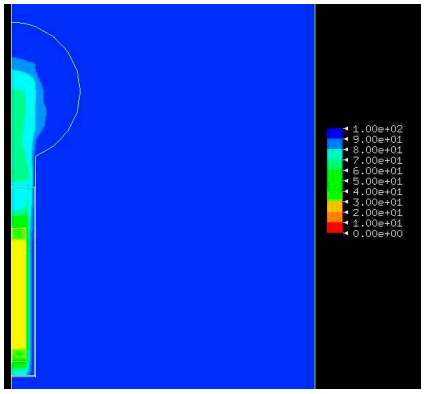	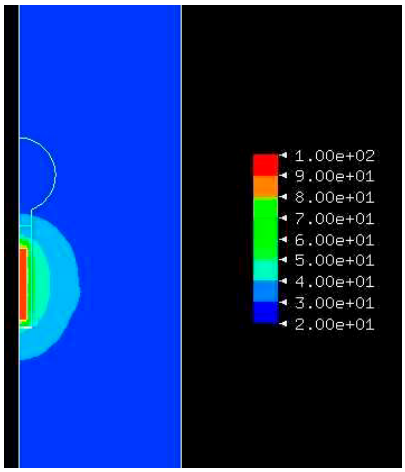
After 5 years	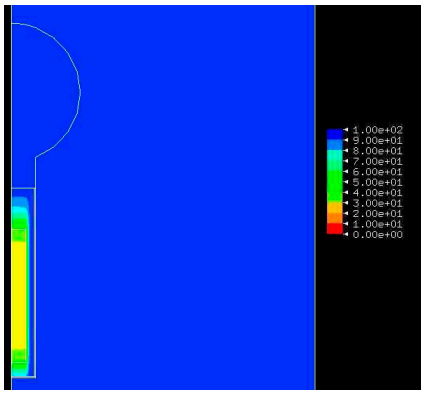	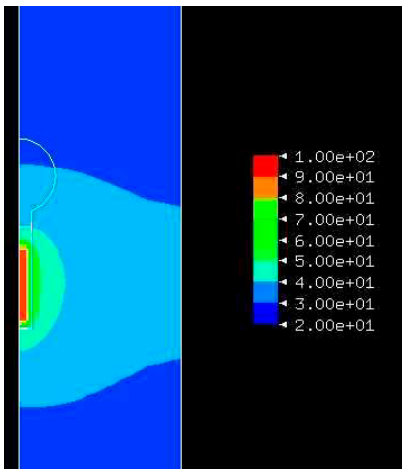

Figure 34 *Distribution of degree of saturation and temperature in buffer and rock (Case1-3)*

Case2-1	Degree of saturation [%]	Temperature [ºC]
After 30 days	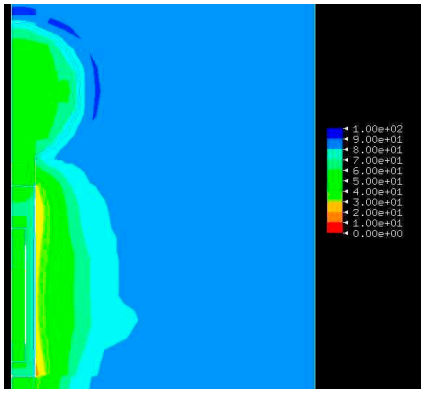	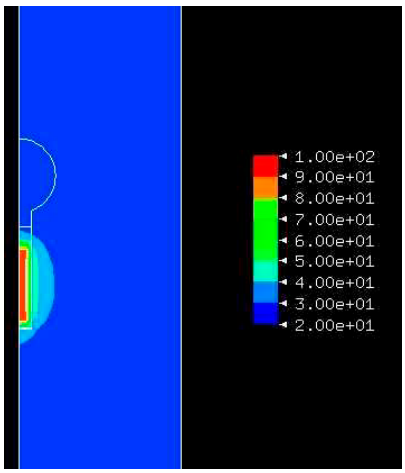
After 1 year	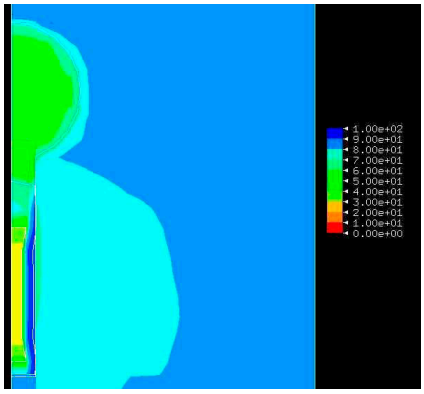	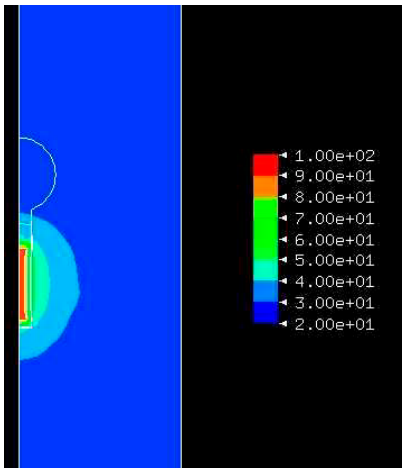
After 5 years	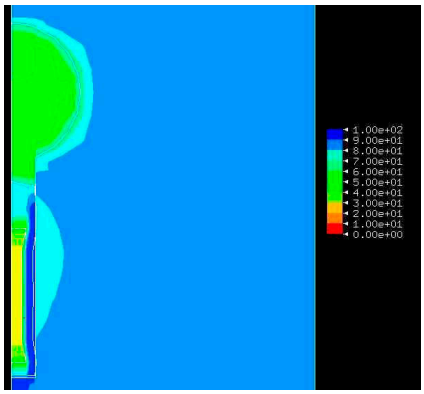	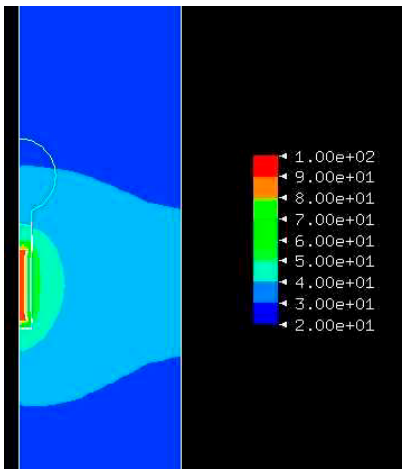

Figure 35 *Distribution of degree of saturation and temperature in buffer and rock (Case2-1)*

Case3-1	Degree of saturation [%]	Temperature [ºC]
After 30 days	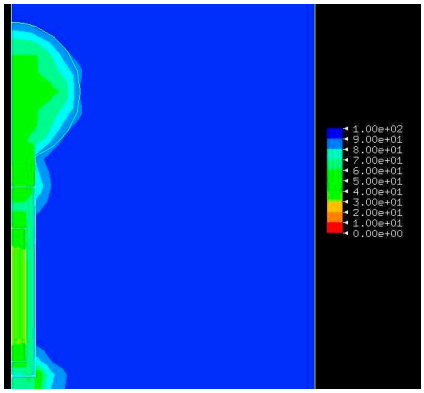	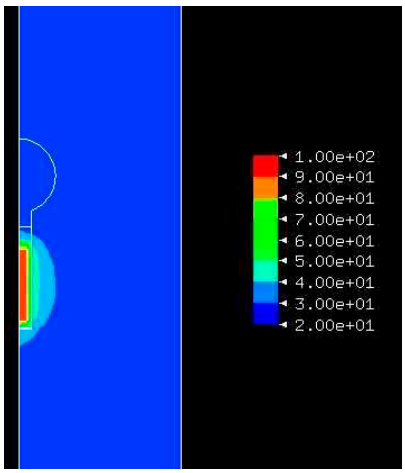
After 1 year	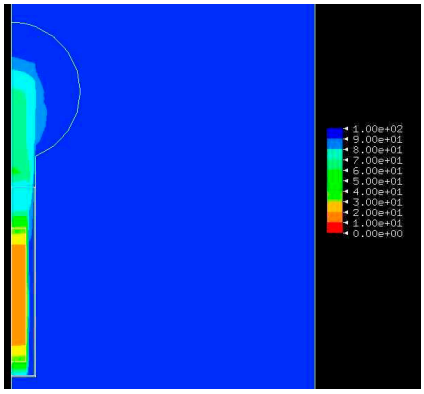	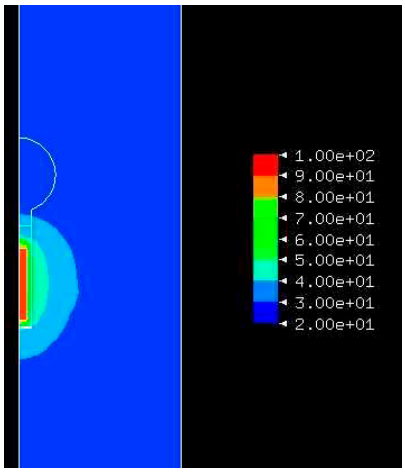
After 5 years	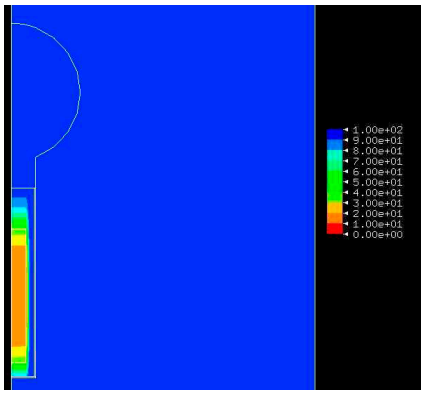	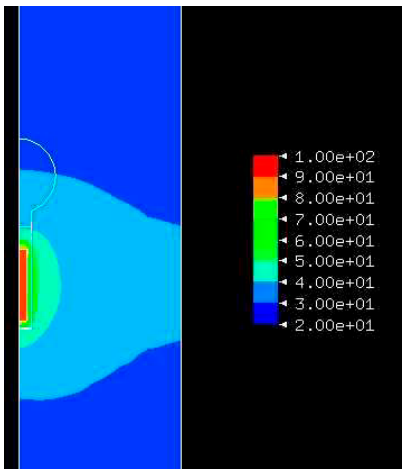

Figure 36 *Distribution of degree of saturation and temperature in buffer and rock (Case3-1)*

Case3-3	Degree of saturation [%]	Temperature [°C]
After 30 days	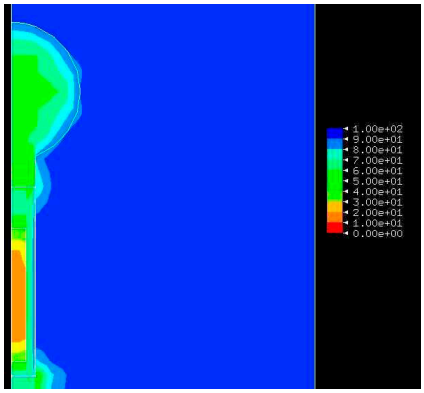	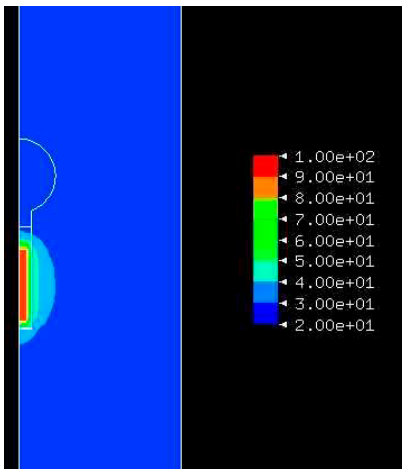
After 1 year	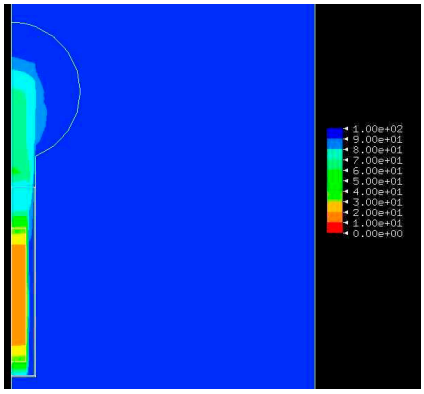	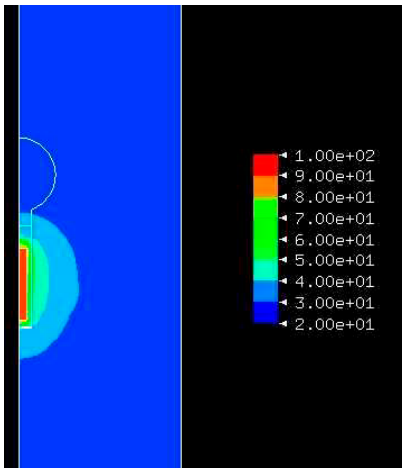
After 5 years	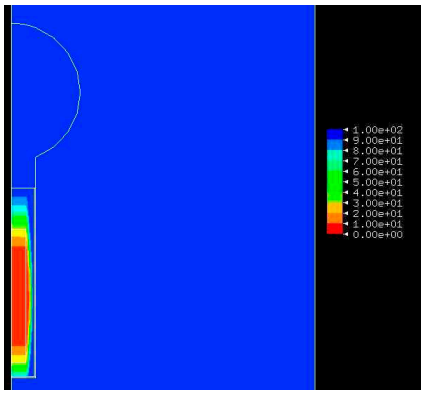	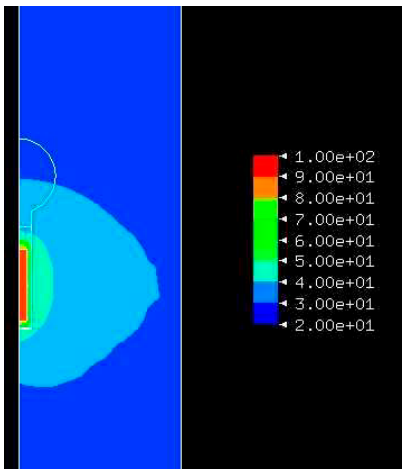

Figure 37 *Distribution of degree of saturation and temperature in buffer and rock (Case3-3)*

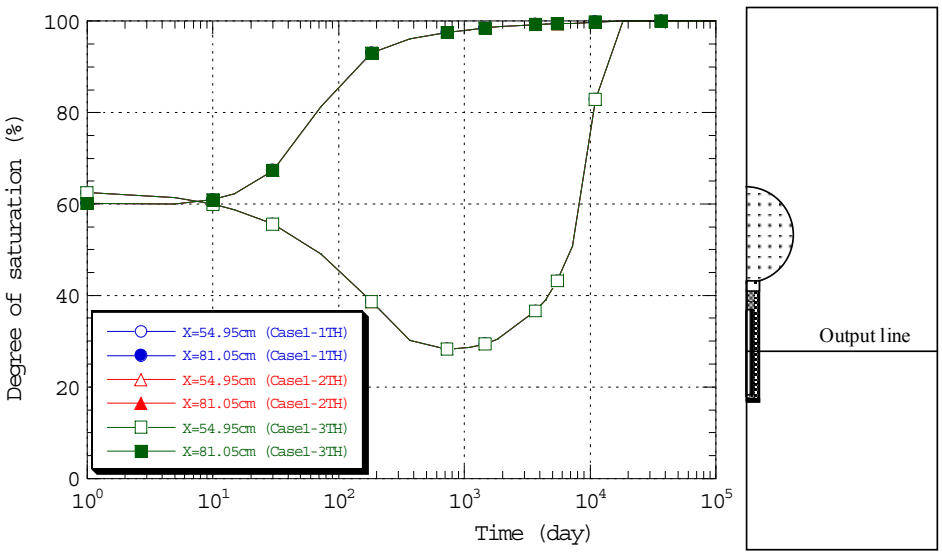

Figure 38 *Comparison of degree of saturation with different permeability of rock mass(Case1)*

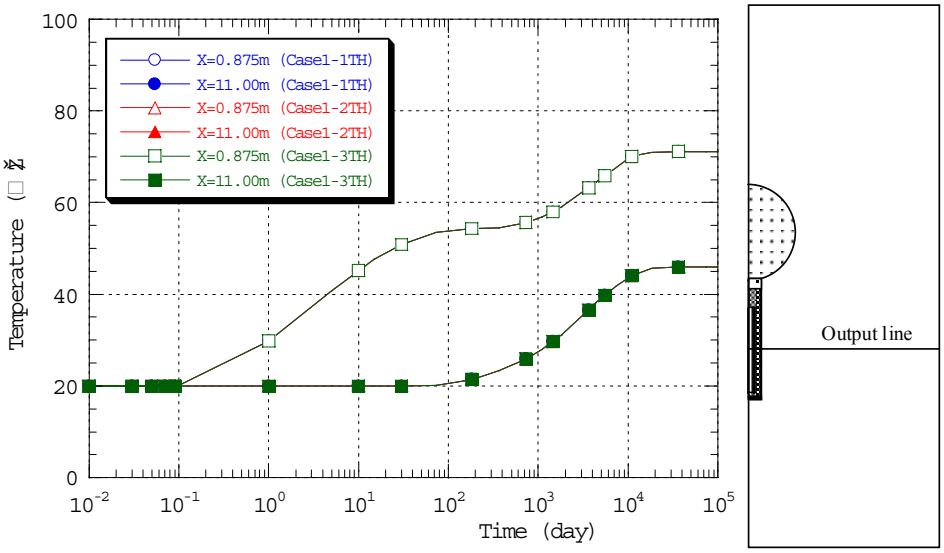

Figure 39 *Comparison of temperature with different permeability of rock mass (Case1)*

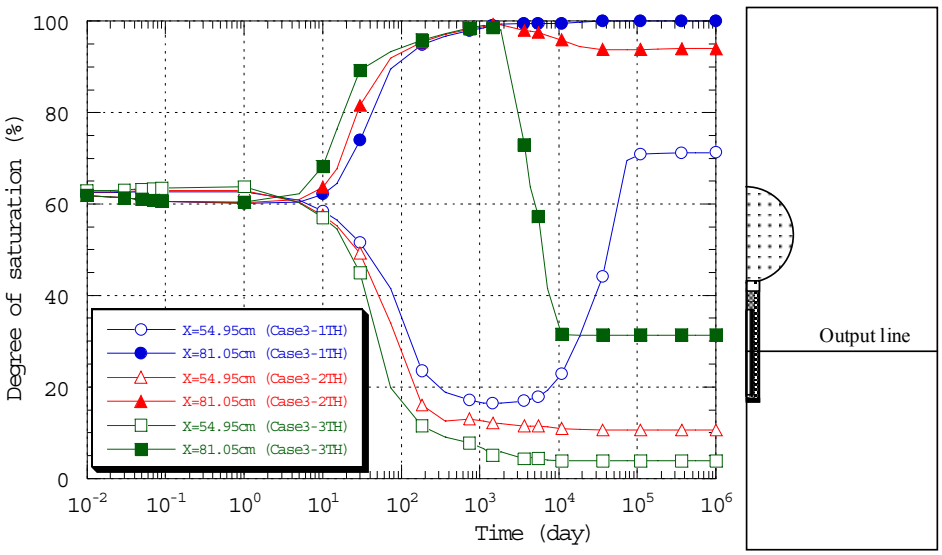

Figure 40 *Comparison of degree of saturation with different thermal vapor flow diffusivity (Case3)*

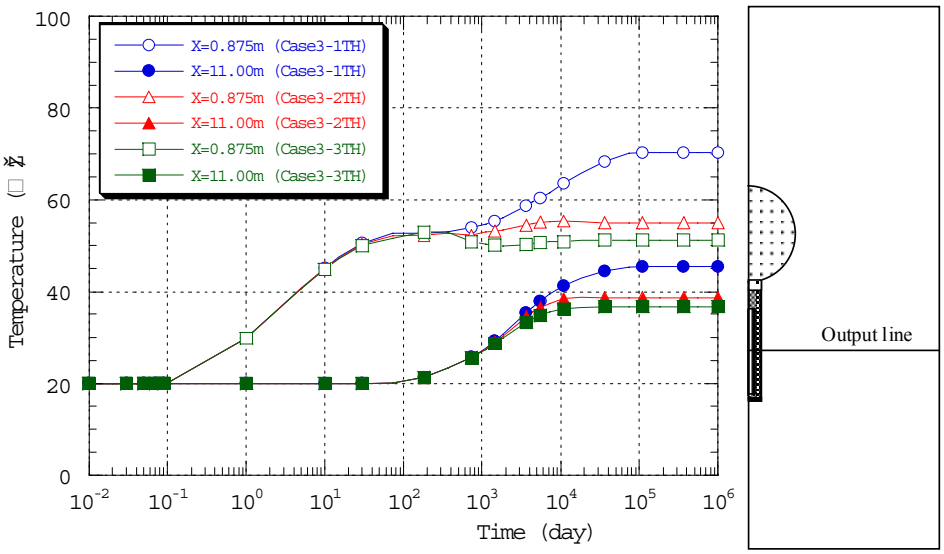

Figure 41 *Comparison of temperature with different thermal vapor flow diffusivity (Case3)*

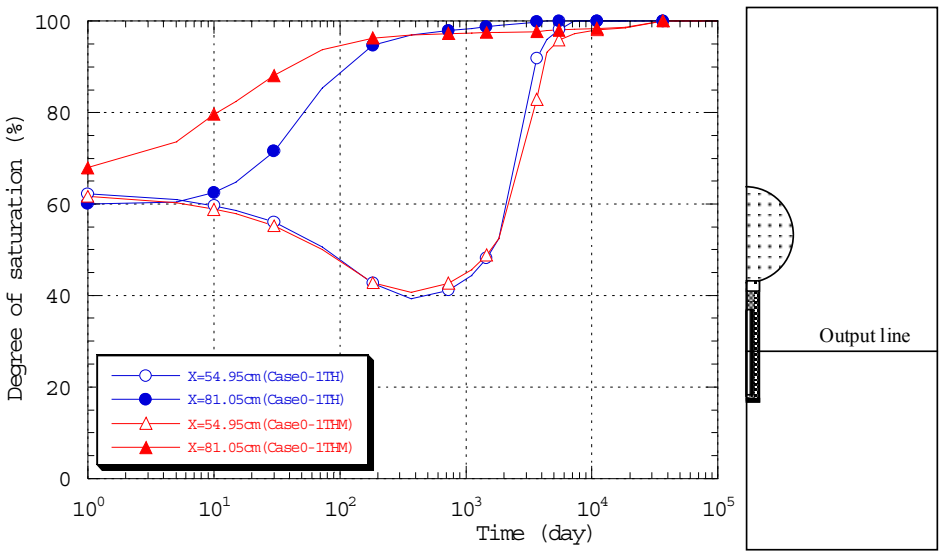

Figure 42 *Comparison of degree of saturation between TH and THM analysis (Case0-1)*

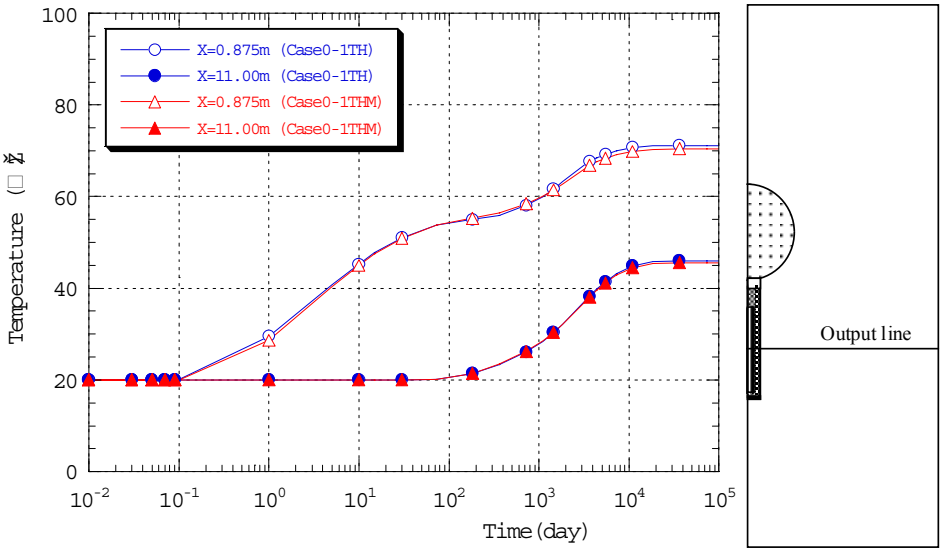

Figure 43 *Comparison of temperature between TH and THM analysis (Case0-1)*

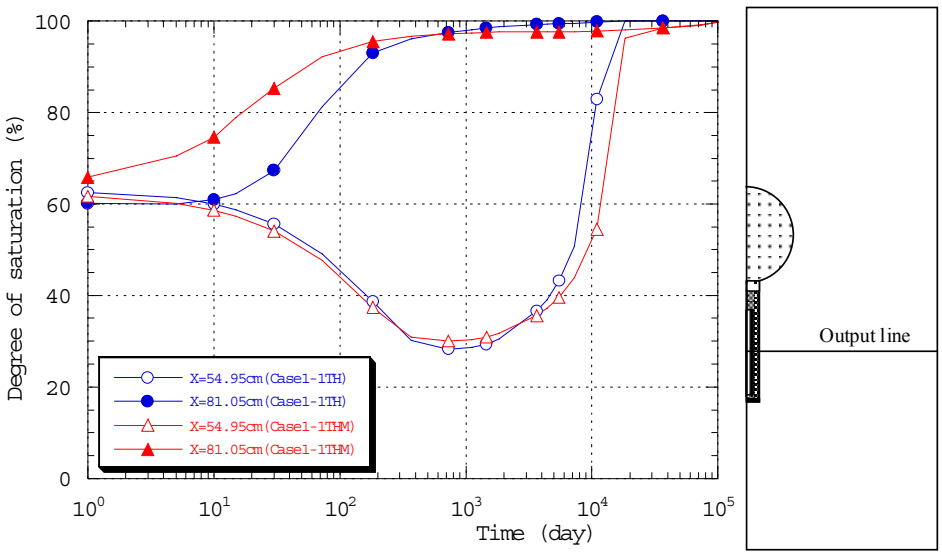

Figure 44 *Comparison of degree of saturation between TH and THM analysis (Case1-1)*

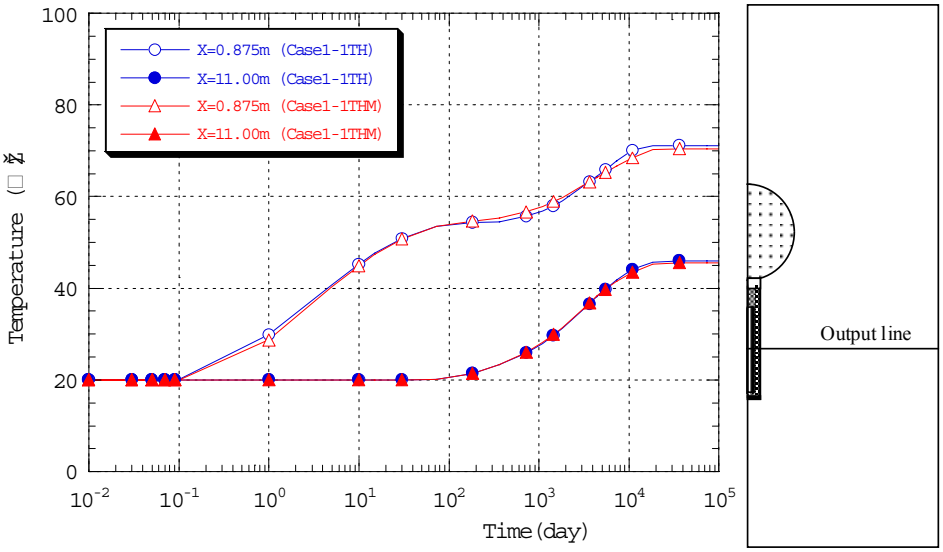

Figure 45 *Comparison of temperature between TH and THM analysis (Case1-1)*

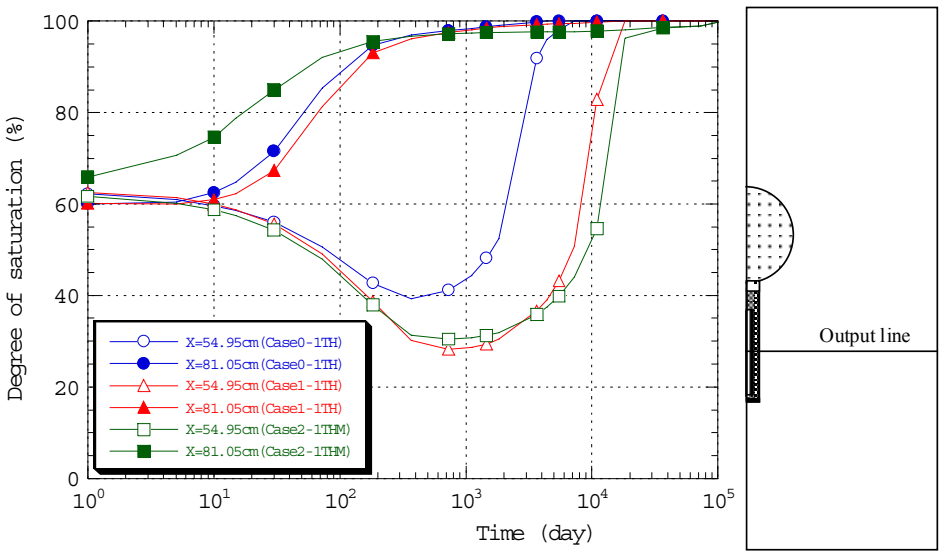

Figure 46 *Comparison of degree of saturation with different model for gap (TH analysis ; Case0-1, 1-1, THM Analysis ; Case 2-1)*

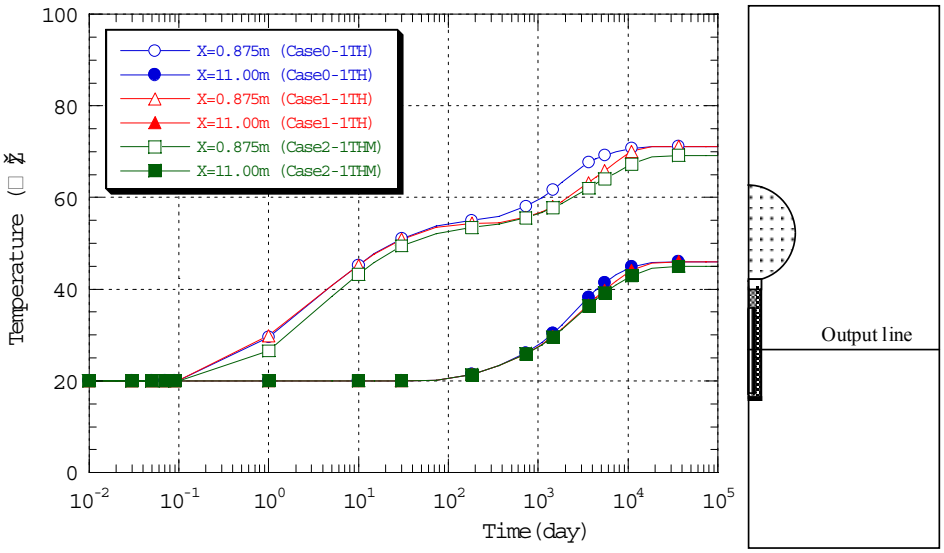

Figure 47 *Comparison of temperature with different model for gap (TH analysis ; Case0-1, 1-1, THM Analysis ; Case 2-1)*

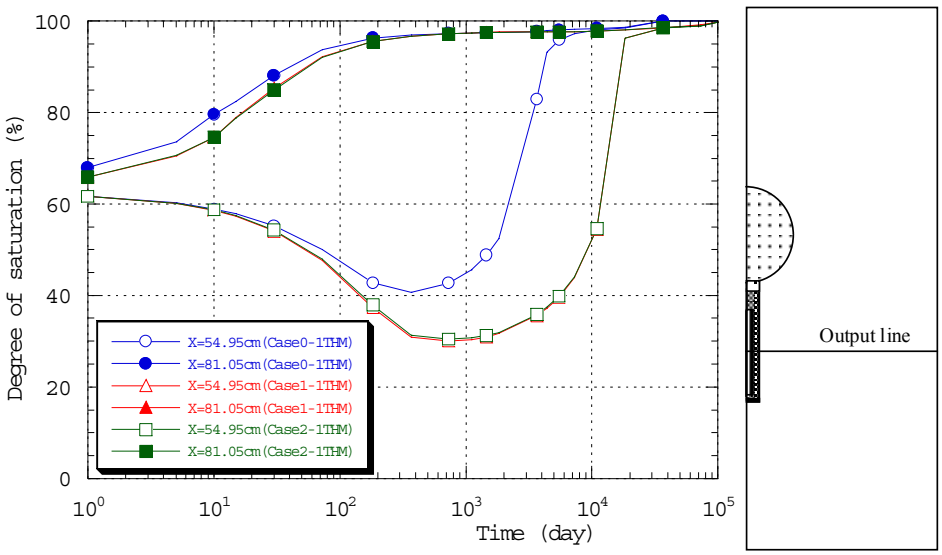

Figure 48 *Comparison of degree of saturation with different model for gap (THM analysis ; Case 0-1, 1-1, 2-1)*

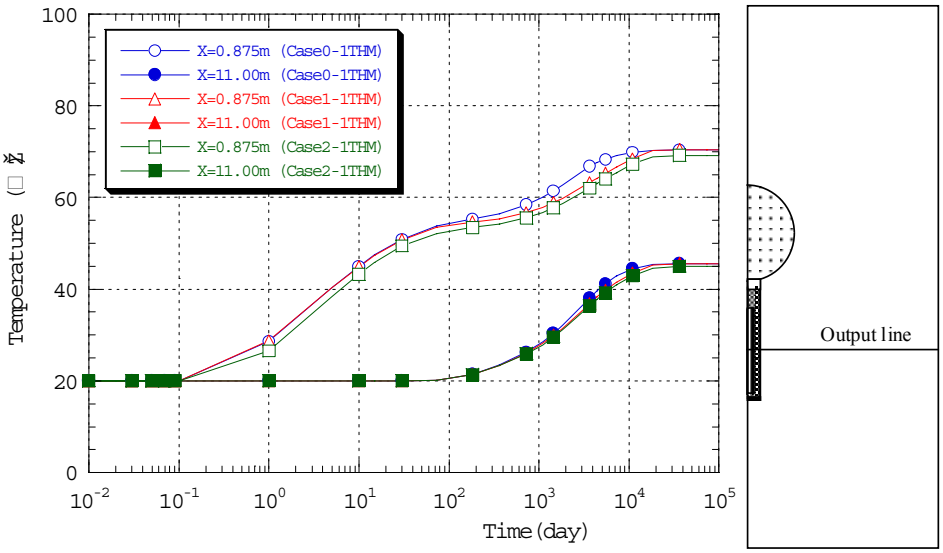

Figure 49 *Comparison of degree of saturation with different model for gap (THM analysis ; Case 0-1, 1-1, 2-1)*

Reference

Börgesson, L. and Hernelind, J. (1999): Preliminary modeling of the water-saturation phase of the buffer and back fill material, SKB IPR-00-11.

Chijimatsu, M., Fujita, T., Kobayashi, A. and Nakano, M. (1998): Calibration and Validation of Thermal, Hydraulic and Mechanical Model for Buffer Material, JNC Technical report JNC TW8400 98-017.

Chijimatsu, M., Fujita, T., Kobayashi, A. and Nakano, M. (2000a): Experiment and validation of numerical simulation of coupled thermal, hydraulic and mechanical behaviour in the engineered buffer materials, Int. J. for Numer. Anal. Meth. Geomech, 24, pp.403-424.

Chijimatsu, M., Fujita, T., Sugita, Y., Amemiya, K. and Kobayashi, A. (2000b): Field experiment, results and THM behavior in the Kamaishi mine experiment, Int. J. of Rock Mec. & Min. Sci., 38, pp. 67-78.

Komine, H. and Ogata, N. (1994): Experimental study swelling characteristics of compacted bentonite, Canadian Geotechnical Journal, 31: pp.478 - 490.

Ohnishi, Y., Shibata, H. and Kobayashi, A. (1985): Development of finite element code for the analysis of coupled thermo-hydro-mechanical behaviors of a saturated-unsaturated medium, Proc. of Int. Symp. on Coupled Process Affecting the Performance of a Nuclear Waste Repository, Berkeley, pp. 263 - 268.

Pusch, R. (1980a): Water uptake, migration and swelling characteristics of unsaturated and saturated, highly compacted bentonite, Swedish Nuclear Fuel Supply Co./Division KBS, Technical Report 80-11.

Pusch, R. (1980b): Swelling pressure of highly compacted bentonite, Swedish Nuclear Fuel Supply Co./Division KBS, Technical Report 80-13.